CRREL
REPORT 83-23

US Army Corps of Engineers
Cold Regions Research & Engineering Laboratory

Stress measurements in ice

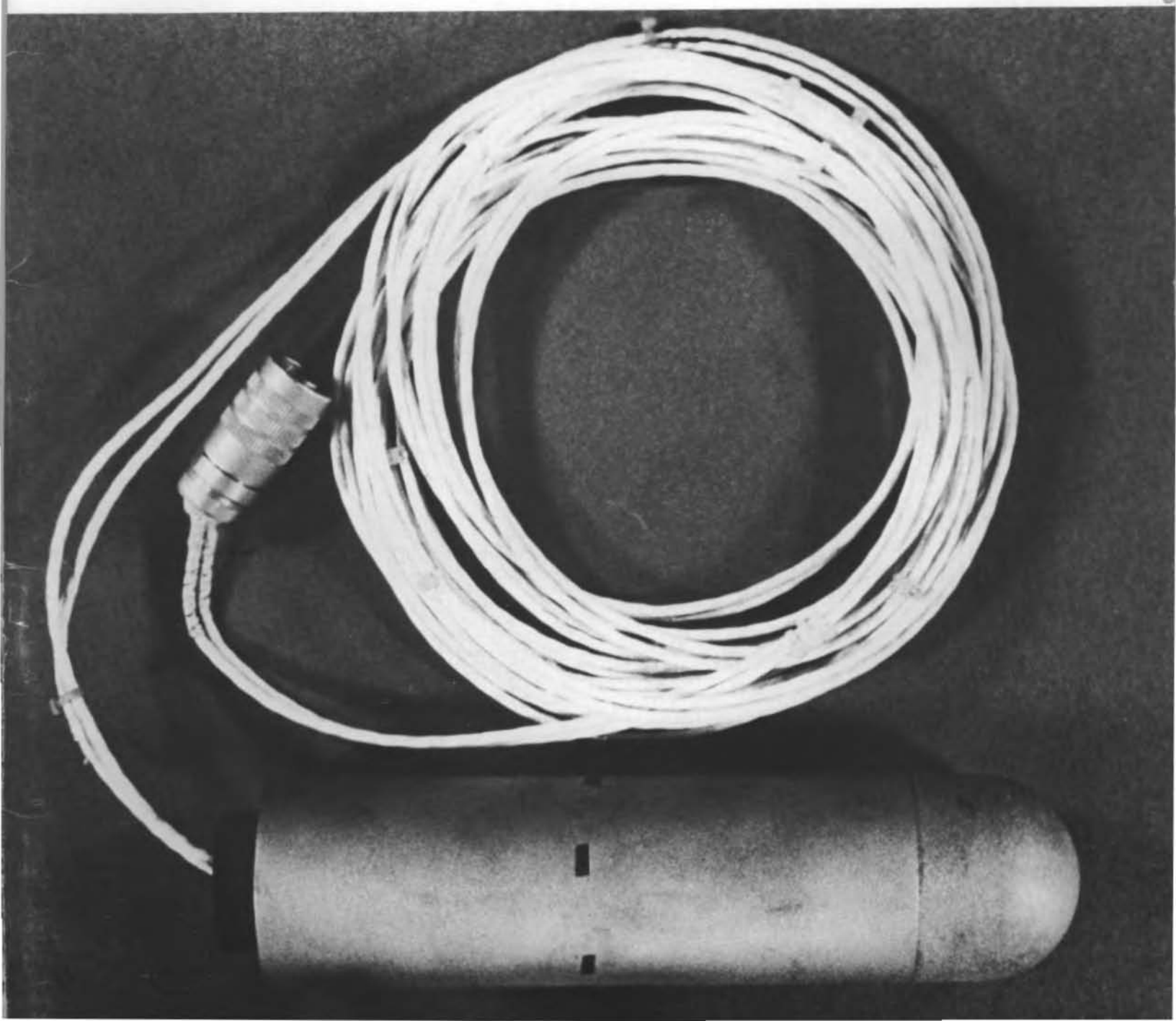

CRREL Report 83-23

August 1983

Stress measurements in ice

Gordon F.N. Cox and Jerome B. Johnson

Approved for public release; distribution unlimited

Unclassified

SECURITY CLASSIFICATION OF THIS PAGE (When Data Entered)

REPORT DOCUMENTATION PAGE		READ INSTRUCTIONS BEFORE COMPLETING FORM
1. REPORT NUMBER CRREL Report 83-23	2. GOVT ACCESSION NO.	3. RECIPIENT'S CATALOG NUMBER
4. TITLE (and Subtitle) STRESS MEASUREMENTS IN ICE		5. TYPE OF REPORT & PERIOD COVERED 6. PERFORMING ORG. REPORT NUMBER
7. AUTHOR(s) Gordon F.N. Cox and Jerome B. Johnson		8. CONTRACT OR GRANT NUMBER(s) U.S.D.I Order No. 2LA6000-1088
9. PERFORMING ORGANIZATION NAME AND ADDRESS U.S. Army Cold Regions Research and Engineering Laboratory Hanover, New Hampshire 03755		10. PROGRAM ELEMENT, PROJECT, TASK AREA & WORK UNIT NUMBERS ILIR 4A161101A91D, Task 00, Work Unit 388
11. CONTROLLING OFFICE NAME AND ADDRESS U.S. Army Cold Regions Research and Engineering Laboratory, Hanover, New Hampshire 03755 and Minerals Management Service, U.S. Department of Interior, Reston, Virginia 22091		12. REPORT DATE August 1983 13. NUMBER OF PAGES 38
14. MONITORING AGENCY NAME & ADDRESS (if different from Controlling Office)		15. SECURITY CLASS. (of this report) Unclassified 15a. DECLASSIFICATION/DOWNGRADING SCHEDULE

16. DISTRIBUTION STATEMENT (of this Report)

Approved for public release; distribution unlimited.

17. DISTRIBUTION STATEMENT (of the abstract entered in Block 20, if different from Report)

18. SUPPLEMENTARY NOTES

19. KEY WORDS (Continue on reverse side if necessary and identify by block number)

Cold regions
Ice
Ice stress
Laboratory tests
Stress sensors

20. ABSTRACT (Continue on reverse side if necessary and identify by block number)

The problems associated with measuring stresses in ice are reviewed. Theory and laboratory test results are then presented for a stiff cylindrical sensor made of steel that is designed to measure ice stresses in a biaxial stress field. Loading tests on freshwater and saline ice blocks containing the biaxial ice stress sensor indicate that the sensor has a resolution of 20 kPa and an accuracy of better than 15% under a variety of uniaxial and biaxial loading conditions. Principal stress directions can also be determined within 5°. The biaxial ice stress sensor is not significantly affected by variations in the ice elastic modulus, ice creep or differential thermal expansion between the ice and gauge. The sensor also has a low temperature sensitivity (5 kPa/°C).

DD FORM 1 JAN 73 1473 EDITION OF 1 NOV 65 IS OBSOLETE

Unclassified

SECURITY CLASSIFICATION OF THIS PAGE (When Data Entered)

PREFACE

This report was prepared by Dr. Gordon F.N. Cox, Geophysicist, of the Snow and Ice Branch, Research Division, U.S. Army Cold Regions Research and Engineering Laboratory and Dr. J.B. Johnson, Geophysicist, Geophysical Institute, University of Alaska. The work was jointly supported by the Minerals Management Service of the U.S. Department of the Interior, Order No. 2LA6000-1088, *Development and Testing of a Field Ice Stress Measurement System,* and the U.S. Army Cold Regions Research and Engineering Laboratory, In-House Laboratory Independent Research, ILIR, DA Project 4A161101A91D, Task 00, Work Unit 388, *Ice Stress Meter.*

The authors appreciate the assistance provided by Nancy Perron, Steve Decato and Bill Bosworth in growing and handling the large ice blocks, as well as preparing ice thin sections. Larry Gould designed the biaxial loading machine which was then fabricated by Bill Burch. The authors also thank Dr. Dev Sodhi of CRREL and Dr. Piyush Dutta of IRAD Gage for technically reviewing the manuscript of this report.

The contents of this report are not to be used for advertising or promotional purposes. Citation of brand names does not constitute an official endorsement or approval of the use of such commercial products.

CONTENTS

ILLUSTRATIONS

TABLES

STRESS MEASUREMENTS IN ICE

Gordon F.N. Cox and Jerome B. Johnson

INTRODUCTION

Reliable, inexpensive ice stress measurements are needed to solve a variety of ice related problems. These include: measuring and monitoring ice loads on marine and hydraulic structures; determining the magnitude of ice forces associated with ice drift, ride-up, pile-up and pressure ridge formation; measuring thermal ice pressures in reservoirs; and assessing the effects of ice convergence on the performance of large icebreakers and tankers.

Researchers have obtained estimates of ice loads on structures by considering the failure strength of the ice; however, because of the uncertainty in the large scale mechanical properties of the ice sheet, these estimates may be too conservative. In situ measurements of stress in ice are needed to accurately determine ice loads on structures.

In this report we first review the problems of measuring ice stress, together with the findings and accomplishments of other investigators who have worked on the development of ice stress sensors. We then present theory and laboratory test results for a stiff steel cylindrical sensor designed to measure ice stresses in a biaxial stress field.

PREVIOUS WORK

Stress measurements

The general problems of measuring stresses in ice and other materials have been adequately addressed by Metge et al. (1975). Stress in any material cannot be measured directly. It must be determined by measuring the strain deformation of the material or by measuring the strain of an elastic inclusion embedded in the medium. In materials that deform elastically and where the elastic modulus is known, the stress can be calculated given the material deformation and elastic modulus. However, in materials such as ice, which exhibit time-dependent deformation and wide variations in the elastic modulus, an imbedded inclusion must be used to measure the stress where the stress-strain relationship and the inclusion factor of the sensor are known. The inclusion factor is defined as the ratio of the undisturbed ice pressure to the pressure felt by the sensor. It should be noted that the elastic modulus of ice can vary over one order of magnitude, from 0.7 to 10 GPa, depending on the ice salinity, temperature, grain size, crystal orientation and strain or loading rate (Traetteberg et al. 1975, Vaudrey 1977, and Schwarz and Weeks 1977).

If the elastic modulus of the inclusion or stress sensor is different than that of the surrounding ice, the sensor will change the local stress field in the ice. A sensor that is stiffer than the ice will support some of the load that would otherwise be supported by the surrounding ice. It will concentrate the stress. If it is softer than the ice it will deflect easily, requiring the surrounding ice to support more of the load. In addition to the relative stiffness between the sensor and the ice, the inclusion factor of the sensor depends on the inclusion geometry and direction of the applied stress in the ice. Hence, precise knowledge of the strain in the sensor, the stress-strain relationship of the sensor material and the inclusion factor are needed to obtain the stress in the ice. The main problem is to determine the inclusion factor and to design the sensor in such a way that it remains nearly constant, even if the ice properties change. In the design of ice stress sensors, variations in ice modulus can be dealt with by either selection of a thin, wide sensor (Metge et al. 1975, Templeton 1979) or a sensor that is much stiffer than the ice (Nelson et al. 1977, Johnson and Cox 1980).

Other potential problems in measuring ice stress, cited in part by Metge et al. (1975) and elaborated by Templeton (1979), include the effects of nonelastic behavior, differential thermal expansion between the ice and the gauge, and overloading of the surrounding ice. Two examples of nonelastic behavior include ice creep and localized plastic yielding around the sensor. Creep tends to reduce the elastic modulus of the ice and to increase its variability. Localized plastic yielding around the sensor may produce deformation in the sensor that remains even after the applied or far-field stress is removed. Differential thermal expansion between the ice and sensor takes place whenever the system temperature changes. This may result in anomalous stress readings entirely caused by the different thermal expansion characteristics between the ice and gauge. If the sensor produces a high stress concentration in the surrounding ice, overloading of the ice may result in localized failure of the ice around the sensor and further stress measurement errors. Templeton (1979) suggests that all these problems can be minimized by the choice of a thin, wide sensor having a modulus close to that of ice. Johnson and Cox (1980) also demonstrated that these problems are not apparent for stiff cylindrical sensors.

Design considerations

In light of the previous discussion and recommendations by Templeton (1979), the following are important design considerations for an ice stress sensor:

1. The sensor should not be affected by variations in the ice elastic modulus and by nonelastic behavior of the ice.
2. The sensor should have a low temperature sensitivity and not be significantly affected by differential thermal expansion.
3. The sensor should not greatly overload the ice.
4. The sensor should be appropriately sized and be rugged and leakproof.
5. The sensor should be inexpensive, easily installed and monitored, and have a stable, repeatable response.

Numerous attempts have been made to design such a sensor. They are described below.

Stress sensors

Ice stress sensors have been developed by Esso Resources Canada (formerly Imperial Oil Limited, IOL), the University of Alaska, Exxon Production Research (EPR), the National Research Council of Canada (NRC) and Oceanographic Services Inc. (OSI) in cooperation with IRAD Gage. Hawkes (1969b) also used a photoelastic stressmeter to measure stresses in frozen sands and Baumann (1979) used earth pressure cells to measure stresses in river ice. These sensors vary widely in geometry and modulus.

The IOL sensor described by Metge et al. (1975) is a thin, wide, soft sensor having an effective elastic modulus less than that of ice. It consists of a double sandwich of aluminum plates and elastomeric material that deforms under applied stress. The amount of deformation is determined

by measurement of the change in capacitance between the metal plates. The gauge is 0.79 cm thick, 122 cm wide and is designed to extend through the full thickness of an ice sheet. The gauge has been widely used by IOL to measure the ice stress around man-made fill islands in Mac-Kenzie Bay.

The University of Alaska gauge is described by Nelson et al. (1977). It consists of a 2.54-cm-diameter aluminum cylinder that is 7.62 cm long, with a 5.08-cm-long by 1.27-cm-diameter reduced section. Four strain gauges, parallel and perpendicular to the axis of the cylinder, are connected in a bridge to read tension or compression in the bar and provide temperature compensation. The aluminum cylinder fits inside a copper tube and has 1.27-cm-diameter steel bolts on each end to grip the ice. The copper tube is sealed to the aluminum bar with silicone rubber and the entire assembly is coated with silicone rubber. Both aluminum and brass have been used to construct the gauge. The dimensions of the gauge have also been slightly modified in various field measurement programs.

The University of Alaska gauge is frozen into the ice horizontally and stresses are measured at the ends of the cylinder. It is a uniaxial device, in that it can only accurately measure ice stress when oriented parallel to a uniaxial stress field. In such an orientation the gauge has an average inclusion factor of 1:3.2. Other tests have shown the sensor to have a transverse sensitivity of up to 25% of the applied load. We should point out that because the off-axis loading characteristics of the gauge have not yet been fully evaluated, measurements in biaxial stress fields only provide an indication of the state of stress, not values of the magnitude and direction of the principal stresses. In uniaxial stress fields, when the gauge is oriented at some angle to the applied stress, the results also have to be carefully interpreted. Nevertheless, the gauge has been successfully used to help understand the general magnitude of the stresses in ice around man-made and natural structures (Sackinger and Nelson 1979a, b, Nelson and Sackinger 1976).

The EPR ice pressure sensor consists of a thin, wide panel that extends through the full thickness of the ice sheet (Templeton 1979). It is 1.11 cm thick and about 45 cm wide. Aluminum sensors with strain gauges are used to measure ice pressures normal to the panel. Constructed sensors have exhibited an effective elastic modulus of up to 1.84 GPa, close to that of sea ice.

Numerous analytical studies have been performed to determine the inclusion factor, transverse sensitivity and differential thermal expansion characteristics of the EPR pressure sensor. Chen (1981a) shows that the average inclusion factor of the gauge is close to 1:1. Chen's elastic finite element analyses also show that the gauge produces a maximum stress concentration factor of 1.5 in the ice near the panel's edge. Other finite element analyses performed by Chen (1981b), using an elastic-plastic ice model, indicate that the sensor has a very low transverse sensitivity. Transverse pressures up to 1.66 MPa result in maximum anomalous pressure on the sensing face of only 0.17 MPa. He found transverse pressure effects to be greatest at small transverse pressures.

In addition to these studies, Templeton (1981) conducted an elasto-static analysis to determine the gauge's sensitivity to differential thermal expansion between the ice and gauge. His results show that errors from differential thermal expansion are independent of the sensor's elastic modulus and can be minimized by choosing a thin, wide sensor. He concludes that errors due to transverse pressures and differential thermal expansion total less than 10% of the measurement.

Chen (1981a) and Chen and Templeton (1983) also present some results of field verification tests on the EPR ice pressure sensor. In these tests the sensor was frozen into large sea ice blocks measuring 3 by 6 m by the full thickness of the ice sheet. The blocks were loaded using two 0.45-MN-capacity hydraulic cylinders. The test results showed that the measured stress was within 15% of the nominal anticipated response for all applied ice pressures greater than 0.69 MPa. At pressures less than 0.69 MPa, the actual response of the gauge was much less than predicted. No field tests have been made to verify the analytical studies of the sensor's transverse sensitivity.

Earth pressure cells have also been used to monitor stresses in ice. Baumann (1979) used Terra-Technology earth pressure cells to measure ice stresses in the St. Marys River, Michigan. The cells

consist of two sealed 20- by 30- by 1-cm steel plates filled with hydraulic fluid which, in turn, is pressurized by CO_2 gas. Pressures are monitored with a gas regulator. The sensors have a sensitivity of 690 Pa and an operating range of 0 to 1.36 MPa. Baumann calibrated the cells in the laboratory; however, he does not give details of the calibration procedure. As no attempt was made to determine the transverse sensitivity of the cells in ice, measurements of stress need to be carefully interpreted, as with the University of Alaska gauge.

The NRC gauge is a thin-walled aluminum tube having an outside diameter of 5.0 cm, a wall thickness of 0.3 cm and a length of 10.0 cm. Three strain gauges are circumferentially bonded to the inside of the tube at 120° intervals to measure the tube deformation under stress. The stresses on the tube are calculated from the circumferential strains, assuming that the ice behaves as a linear elastic material (Frederking 1980).

The tube material and dimensions are chosen to minimize the stress and strain distributions in the surrounding ice associated with the presence of the sensor. The displacements of the outer diameter of the tube approximate those of a solid ice cylinder of the same size. In effect, the gauge has an inclusion factor close to 1:1.

Both laboratory and field tests of the NRC gauge show that a tubular transducer can successfully be used to determine the principal stress direction. This agrees with the theory presented by Frederking. In calibration tests where the elastic modulus of the ice was known, the measured principal stresses were within 20% of the applied stress. In the field, poorer agreement was obtained; however, this was in part due to the uncertainty in the applied stress field.

Calculations presented later in this report show that the inclusion factor of a cylindrical inclusion, having an effective modulus close to that of ice, is very sensitive to small changes in the ice modulus. If the ice creeps, resulting in a large decrease in the effective ice modulus, significant errors can be expected with this type of sensor.

The OSI sensor described by Johnson and Cox (1980) is similar to the NRC gauge in that it also is a cylindrical inclusion. The sensor has an outer diameter of 2.86 cm, a wall thickness of 0.79 cm and a length of 57.0 cm. The ends of the gauge are fitted with rounded end caps. Relative to the NRC gauge, this sensor is much stiffer, having an effective elastic modulus much greater than that of ice.

The ice stress is determined by monitoring the radial deformation of the cylinder with a vibrating wire (Hawkes and Bailey 1973). Savin's (1961) stress-deformation relations for cylindrical elastic inclusions in elastic and viscoelastic materials are used to calculate the applied stresses from the radial deformation of the gauge. Three sensors, oriented 45° to one another, are used in the field to measure the magnitude and direction of the principal stresses in the ice sheet.

The gauge response was evaluated in the laboratory by freezing the sensor into a block of ice and applying a known uniaxial load. Measured stresses were generally within 10% of the applied stress for loads up to 2.1 MPa and ice block strains less than 0.25%. In long-term creep tests where block strains of 4% were obtained, measured stresses were within 20% of the applied stress. The gauge response was not significantly affected by variations in the ice modulus, creep and differential thermal expansion between the ice and gauge. The sensor also had a low temperature sensitivity.

Hawkes (1969b) used a rigid photoelastic stressmeter to measure stresses in blocks of frozen sand. The stressmeter consisted of a 3.81-cm-long glass cylinder having an outside diameter of 3.18 cm and a wall thickness of 1.27 cm. In this technique stresses are determined from isochromatic fringe patterns when the sensor is viewed between crossed polarizers. As these meters had been successfully used in rock and concrete under elastic loads, the objective of Hawkes' experiment was to evaluate the response of the sensor in materials undergoing creep deformation. In his tests the sensor was inserted into blocks of frozen sand under constant load. Measured stresses were found to be within 10% of the applied stress up to block strains of 5%. Stiff cylindrical sensors have also been tested in nonlinear viscoelastic materials under both uniaxial and biaxial

loads (Hawkes 1969b, Skilton 1971, Buswell et al. 1975). Measured stresses were within 2 to 10% of the applied stress for both short-term and long-term loading.

In summary, previous investigations have shown that there are two suitable stress sensor designs for measuring stresses in ice: a stiff cylindrical sensor having an effective modulus much greater than ice, and a thin, wide sensor, preferably having an effective modulus close to that of ice.

BIAXIAL ICE STRESS SENSOR

The remainder of this report deals with the testing and evaluation of a stiff cylindrical sensor, described by Johnson and Cox (1982), that is used to measure ice stresses in a biaxial stress field. It is an extension of the work on uniaxial cylindrical sensors conducted by Johnson and Cox (1980). During the preparation of this report we learned that in 1975, Ivor Hawkes of IRAD Gage suggested to Sun Oil that a stiff cylindrical sensor, equipped with three vibrating wires, could be used to measure the principal stresses in the plane of an ice sheet (Hawkes 1975). As Sun Oil did not pursue Hawkes' suggestion, the development and testing of such a sensor was not carried out until this study.

The sensor considered in this investigation consists of a stiff cylinder made of steel (Fig. 1 and 2). It is 20.3 cm long, 5.7 cm in diameter and it has a wall thickness of 1.6 cm. The ends of the sensor are threaded such that a rounded end cap can be attached to the lower end of the sensor. Extension rods can also be screwed to the top of the sensor to position the sensing portion of the gauge at any desired depth in the ice sheet.

Principal ice stresses normal to the axis of the gauge are determined by measuring the radial deformation of the cylinder wall in three directions. This is accomplished by use of vibrating wire technology advanced by IRAD Gage (Hawkes and Bailey 1973). Three tensioned wires are set 120° from each other across the cylinder diameter (Fig. 2). The diametral deformation of the gauge in these three directions is determined by plucking each wire with a magnet/coil assembly

Figure 1. Biaxial ice stress sensor.

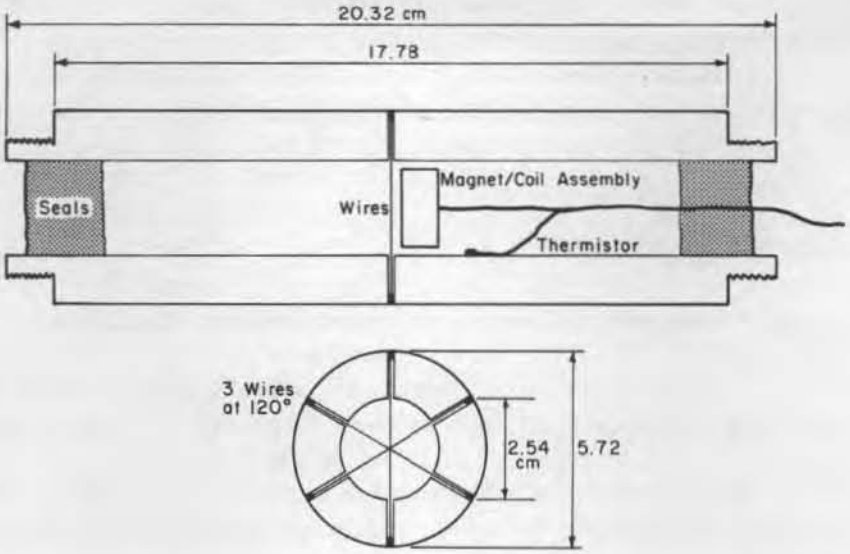

Figure 2. Schematic of biaxial ice stress sensor.

and measuring the resonant frequency of the vibrating wires. A thermistor is also placed inside the cylinder to measure the gauge temperature. Both ends of the sensor are sealed to protect the wires and electronics from moisture. The sensor was fabricated by IRAD Gage in Lebanon, N.H.

This design offers several advantages. The sensor is rugged and leakproof and it can be easily installed in the ice using conventional ice augering equipment. As the sensor output is in terms of frequency, it is not affected by leakage to ground, poor contacts and long lead lengths. The sensor is also inexpensive ($1700 for the prototype, including labor and materials).

BIAXIAL STRESS SENSOR THEORY

The measurement of stresses in an ice sheet with an imbedded sensor requires precise knowledge of the strain in the sensor, the stress-strain relationship of the sensor material and the sensor's inclusion factor under different loading conditions. Fortunately, we know the modulus of the biaxial steel sensor and we can precisely determine the gauge deformation using vibrating wire technology. Analytical solutions are also available that describe the behavior of a cylindrical inclusion in a plate under loading.

Since we are generally interested in compressive stresses in an ice sheet, compressive displacements and stresses are taken to be positive in this report as is often done in rock mechanics. Principal stresses are designated by p and q. The major principal stress, p, is the larger compressive stress, such that $p > q$. All angles are measured clockwise from the p direction.

Gauge deformation

The diametral deformation of the gauge is determined by measuring the resonant frequency of each of the three vibrating wires. The fundamental frequency of each wire is proportional to the strain in the wire and is related to the wire strain by (Halliday and Resnick 1970)

$$f = \frac{1}{2\ell_w} \sqrt{\frac{\epsilon E_w}{\rho_w}} \qquad (1)$$

where

f = natural frequency of the wire (s^{-1})
ℓ_w = wire length (5.08×10^{-2} m)
ϵ = wire strain
E_w = wire modulus (207 GPa)
ρ_w = wire density (7.83×10^3 kg/m^3).

Equation 1 may also be expressed as

$$\epsilon = k f^2$$

or $$\Delta\epsilon = k \Delta(f^2)$$

where
$$k = \frac{4\ell_w^2 \rho_w}{E_w} \tag{2}$$

$$\Delta(f^2) = (f^2 - f_0^2)$$

and f_0 is the initial wire frequency. Since the radial deformation of the cylinder, V_r, at $\ell_w/2$ is equal to

$$V_r = \frac{\ell_w}{2} \Delta\epsilon$$

we have

$$V_r = - \frac{\ell_w}{2} k \Delta(f^2) . \tag{3}$$

Hence, the radial deformation of the cylinder can be expressed in terms of the change in frequency of the vibrating wires.

For our gauge and vibrating wire meter, we can measure radial displacements as small as 5.0×10^{-3} μm (2.0×10^{-7} in.). This corresponds to a sensor resolution of about 20 kPa (3 lbf/in.^{2}) when it is embedded in ice. For the improved vibrating wire meters now under development, the gauge resolution will be increased tenfold. Despite the stiffness of the gauge, it is still very sensitive to loading.

Stresses associated with cylindrical sensors

The stress-deformation relationship for cylindrical elastic inclusions in elastic and viscoelastic materials has been examined both analytically and experimentally. Savin (1961), Berry and Fairhurst (1966), Williams (1973) and others have developed analytical solutions for elastic materials. Experimental tests have verified that the analytical solutions accurately describe the stress distribution in an elastic plate (Suzuki 1969, Wilson 1961). The analytical solutions also describe the deformation of cylindrical elastic inclusions in viscoelastic and other time-dependent materials in uniaxial and biaxial loading experiments (Hawkes 1969a, b, Skilton 1971, Williams 1973, Buswell et al. 1975, Johnson and Cox 1980).

The stress and displacement equations used in this investigation to describe the behavior of the biaxial stress sensor and surrounding ice are based on the work of Savin (1961). Savin (1961) developed a set of analytical equations to describe the behavior of an elastic ring welded in an elastic plate. Even though ice has time-dependent properties, the analytical results of Berry and Fairhurst and the experimental work of Hawkes, Skilton, and Buswell indicate that Savin's

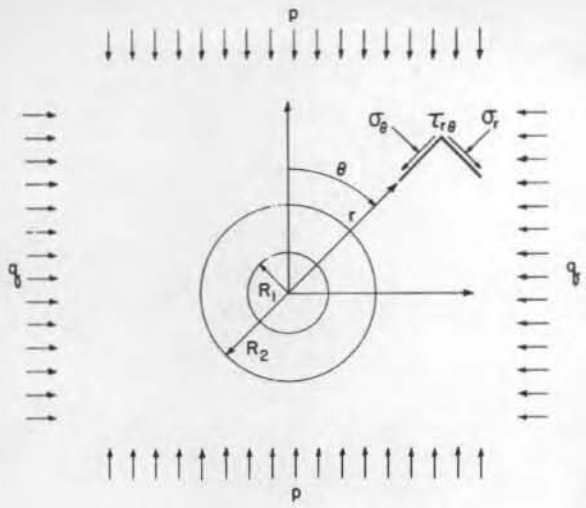

Figure 3. Plan view of cylindrical sensor frozen into ice.

equations can be used in our application. Because the gauge is significantly stiffer than the ice, its response should not be affected by variations or changes in the ice modulus.

Generally, we are interested in measuring in-plane stresses in the ice sheet. Consider a cylindrical sensor that is frozen into an infinite isotropic ice sheet (Fig. 3). The sensor is oriented normal to the plane of the ice sheet, which is subjected to in-plane principal stresses p and q. The sensor has an outer radius R_2 and an inner radius R_1. The stress (σ_r, σ_θ and $\tau_{r\theta}$) and displacement (V_r and V_θ) equations for the sensor ($R_1 \leq r \leq R_2$) in polar coordinates are

$$\sigma_r = \left(\frac{p+q}{2}\right)\left(C_2 - \frac{C_5}{2}\frac{R_2^2}{r^2}\right) + \left(\frac{p-q}{2}\right)\left(\frac{C_7}{2} - 2C_1\frac{R_2^2}{r^2} - \frac{3}{2}C_4\frac{R_2^4}{r^4}\right)\cos 2\theta \tag{4}$$

$$\sigma_\theta = \left(\frac{p+q}{2}\right)\left(C_2 + \frac{C_5}{2}\frac{R_2^2}{r^2}\right) - \left(\frac{p-q}{2}\right)\left(\frac{C_7}{2} - 6C_3\frac{r_2^2}{R_2} - \frac{3}{2}C_4\frac{R_2^4}{r^4}\right)\cos 2\theta \tag{5}$$

$$\tau_{r\theta} = \left(\frac{p-q}{2}\right)\left(3C_3\frac{r^2}{R_2^2} - \frac{C_7}{2} - C_1\frac{R_2^2}{r^2} - \frac{3}{2}C_4\frac{R_2^4}{r^4}\right)\sin 2\theta \tag{6}$$

$$V_r = \frac{(p+q)}{8\mu_s}R_2\left(C_2(X_s-1)\frac{r}{R_2} + C_5\frac{R_2}{r}\right) + \frac{(p-q)}{8\mu_s}R_2\left(C_3(X_s-3)\frac{r^3}{R_2^3} + C_7\frac{r}{R_2} + C_1(X_s+1)\frac{R_2}{r} + C_4\frac{R_2^3}{r^3}\right)\cos 2\theta \tag{7}$$

$$V_\theta = \frac{(p-q)}{8\mu_s}R_2\left(C_3(X_s+3)\frac{r^3}{R_2^3} - C_7\frac{r}{R_2} - C_1(X_s-1)\frac{R_2}{r} + C_4\frac{R_2^3}{r^3}\right)\sin 2\theta. \tag{8}$$

The stress and displacement equations for the ice sheet ($r \geq R_2$) are

$$\sigma_r = \left(\frac{p+q}{2}\right)\left(1 - \frac{C_6}{2}\frac{R_2^2}{r^2}\right) + \left(\frac{p-q}{2}\right)\left(1 - 2C_8\frac{R_2^2}{r^2} - \frac{3}{2}C_9\frac{R_2^4}{r^4}\right)\cos 2\theta \tag{9}$$

$$\sigma_\theta = \left(\frac{p+q}{2}\right)\left(1 + \frac{C_6}{2}\frac{R_2^2}{r^2}\right) - \left(\frac{p-q}{2}\right)\left(1 - \frac{3}{2}C_9\frac{R_2^4}{r^4}\right)\cos 2\theta \tag{10}$$

$$\tau_{r\theta} = -\left(\frac{p-q}{2}\right)\left(1 + C_8\ \frac{R_2^2}{r^2} + \frac{3}{2}\,C_9\ \frac{R_2^4}{r^4}\right)\ \sin 2\theta \tag{11}$$

$$V_r = \frac{(p+q)}{8\mu_i}\ R_2\ \left((X_i - 1)\ \frac{r}{R_2} + C_6\ \frac{R_2}{r}\right)$$

$$+\ \frac{(p-q)}{8\mu_i}\ R_2\ \left(2\ \frac{r}{R_2} + C_8\,(X_i + 1)\ \frac{R_2}{r} + C_9\ \frac{R_2^3}{r^3}\right)\ \cos 2\theta \tag{12}$$

$$V_\theta = \frac{(p-q)}{8\mu_i}\ R_2\ \left(-2\ \frac{r}{R_2} - C_8\,(X_i - 1)\ \frac{R_2}{r} + C_9\ \frac{R_2^3}{r^3}\right)\ \sin 2\theta. \tag{13}$$

The coefficients C_1 through C_9 depend on the sensor geometry and the material properties of the sensor and ice where

$$C_1 = 2\left(\frac{1 + X_i}{D}\right)\left[\left(\frac{\mu_i}{\mu_s} - 1\right) + n^6\left(1 + X_s\,\frac{\mu_i}{\mu_s}\right)\right] \tag{14}$$

$$C_2 = \frac{n^2\,(1 + X_i)}{2\left(\frac{\mu_i}{\mu_s} - 1\right) - n^2\left[\left(\frac{\mu_i}{\mu_s} - 1\right) - \left(1 + X_s\,\frac{\mu_i}{\mu_s}\right)\right]} \tag{15}$$

$$C_3 = -2\ \frac{(1 + X_i)}{D}\ \ n^4\ (n^2 - 1)\left(\frac{\mu_i}{\mu_s} - 1\right) \tag{16}$$

$$C_4 = -2\ \frac{(1 + X_i)}{D}\ \ \left[\left(\frac{\mu_i}{\mu_s} - 1\right) + n^4\ \left(1 + X_s\,\frac{\mu_i}{\mu_s}\right)\right] \tag{17}$$

$$C_5 = \frac{2C_2}{n^2} \tag{18}$$

$$C_6 = 2 - 2\ \frac{(n^2 - 1)}{n^2}\ C_2 \tag{19}$$

$$C_7 = 2\ \frac{(1 + X_i)}{D}\ \ \left[\left(\frac{\mu_i}{\mu_s} - 1\right)(4 - 3n^2) + n^6\ \left(1 + X_s\,\frac{\mu_i}{\mu_s}\right)\right]n^2 \tag{20}$$

$$C_8 = 2 - 2\ \frac{(1 + X_i)}{D}\ \left[\left(\frac{\mu_i}{\mu_s} - 1\right)\ (3n^6 - 6n^4 + 4n^2 - 1) + n^6\,(n^2 - 1)\left(1 + X_s\,\frac{\mu_i}{\mu_s}\right)\right] \tag{21}$$

$$C_9 = -2 + 2\ \frac{(1 + X_i)}{D}\ \ \left[\left(\frac{\mu_i}{\mu_s} - 1\right)\ (4n^6 - 7n^4 + 4n^2 - 1) + n^4\,(n^4 - 1)\ \left(1 + X_s\,\frac{\mu_i}{\mu_s}\right)\right] \tag{22}$$

In the above equations

$$n = \frac{R_2}{R_1}$$

$$\mu = \frac{E}{2(1+\nu)}$$

$$X = \frac{(3-\nu)}{(1+\nu)} \qquad \text{for plane stress}$$

$$X = (3-4\nu) \qquad \text{for plane strain}$$

$$D = \left(X_i + \frac{\mu_i}{\mu_s}\right) n^2 \left[\left(\frac{\mu_i}{\mu_s} - 1\right)(3n^4 - 6n^2 + 4) + n^6\left(1 + X_s \frac{\mu_i}{\mu_s}\right)\right]$$

$$+ \left(X_s \frac{\mu_i}{\mu_s} - X_i\right)\left[\left(\frac{\mu_i}{\mu_s} - 1\right) + n^6\left(1 + X_s \frac{\mu_i}{\mu_s}\right)\right] \qquad (23)$$

E is Young's modulus and ν is Poisson's ratio where the subscripts s and i denote the material properties of the sensor and ice respectively. θ is the angle measured clockwise from the principal stress direction p.

Before we use these equations to compute the ice stress from the radial deformation of the gauge, it is instructive to examine the general behavior of the gauge and ice under different loading conditions. Since the gauge is bonded to the ice, the radial stresses in the gauge and ice are equal at the ice-gauge boundary. Equations 4 or 9 can therefore be used to evaluate the gauge response to variations in the ice modulus. In Figure 4 the normalized radial stress σ_r at the ice-gauge boundary parallel to the uniaxial loading direction p is plotted against the ice-gauge modulus ratio, E_i/E_s. In performing this calculation, we assume plane stress and

$$r = R_2$$

$$\theta = 0^\circ$$

and

$$\nu_i = \nu_s = 0.33.$$

It is apparent from Figure 4 that in situations where the gauge is significantly stiffer than the ice, the gauge response is not appreciably affected by variations in the ice modulus. The ratio σ_r/p remains constant at a value of 1.5. This corresponds to an inclusion factor of 0.67. For the biaxial

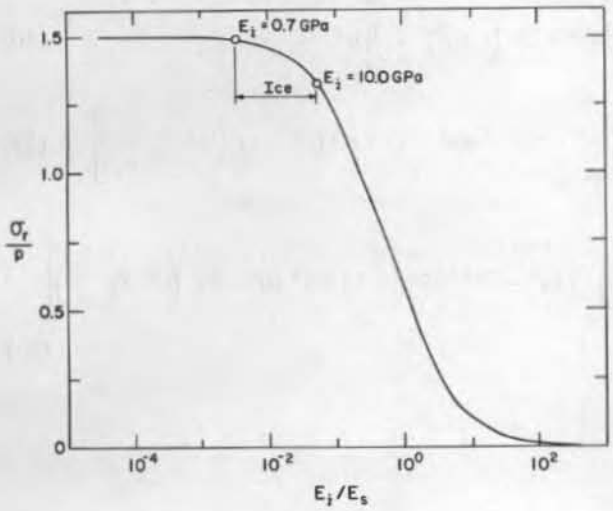

Figure 4. Normalized radial stress at ice-gauge boundary parallel to uniaxial loading direction versus ice-gauge modulus ratio.

ice stress sensor that has a modulus of about 200 GPa, there is a slight variation in the inclusion factor for ice moduli ranging from 0.7 to 10 GPa. However, this can be partially compensated for by selecting an ice modulus appropriate for the type of ice in which the sensor is installed. It should also be noted that creep of the ice reduces the effective ice-gauge modulus ratio and results in only small changes in the inclusion factor.

Frederking (1980) designed a much softer cylindrical ice stress sensor having an "effective" modulus close to that of ice. Even though this design minimizes overloading of the surrounding ice, the sensor response is greatly affected by variations in the ice modulus and creep because it is relatively soft. Frederking obtained poor results in sensor verification tests where the ice modulus was not known.

In addition to variations in the ice modulus, we are also concerned about overloading the surrounding ice when we design ice stress sensors. Figures 5 through 7 give the stress field in the ice surrounding the biaxial ice stress sensor for both uniaxial and biaxial loading conditions. In preparing these plots, we assumed plane stress and chose the ice modulus to be 3.0 GPa.

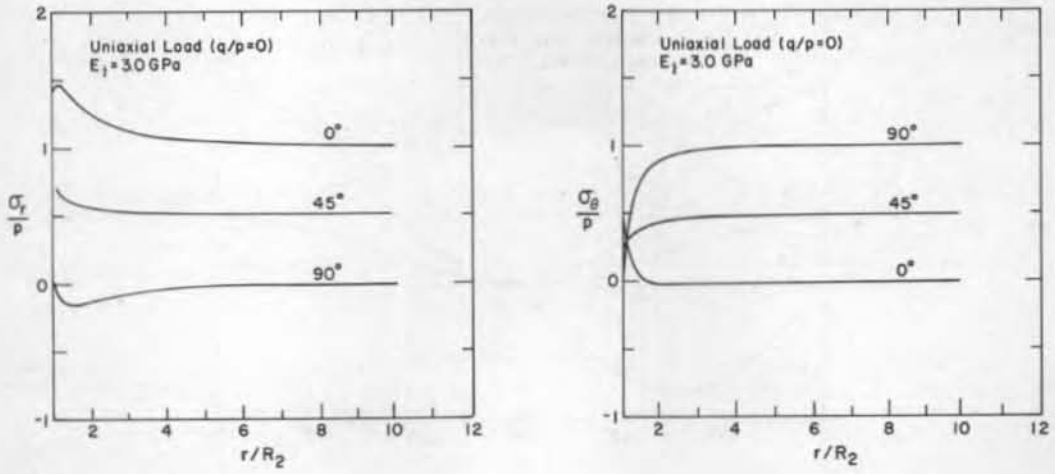

a. Radial stress. *b. Tangential stress.*

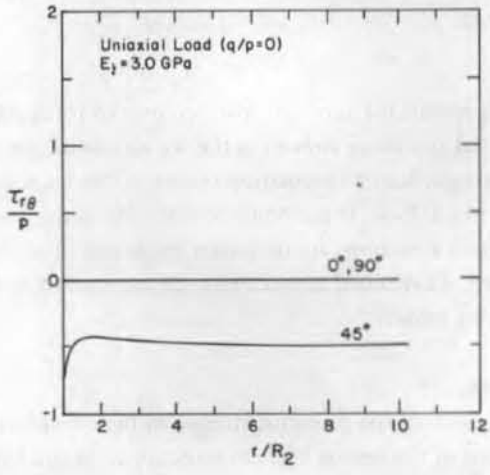

c. Shear stress.

Figure 5. Normalized stress distribution in the ice surrounding the biaxial ice stress sensor under uniaxial loads.

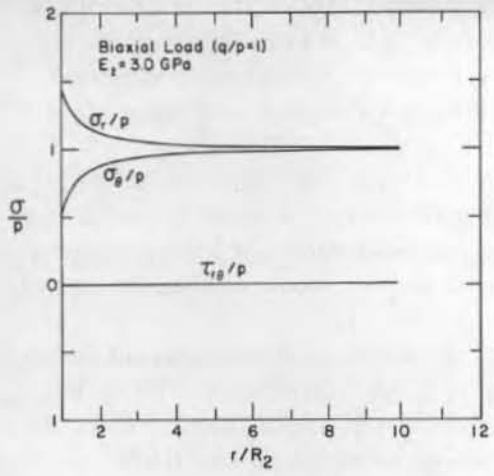

Figure 6. Normalized radial, tangential and shear stress distribution in the ice surrounding the biaxial ice stress sensor under biaxial loads (q/p = 1).

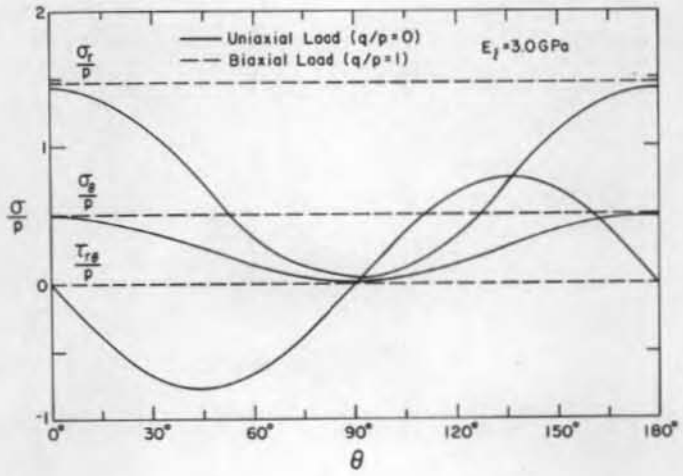

Figure 7. Normalized radial, tangential and shear stress distribution in the ice at the ice-gauge boundary under uniaxial and biaxial loads.

Examination of these plots reveals the possible shortcomings of using stiff cylindrical stress sensors in ice. Radial, tangential and shear stresses in the ice can be increased by 50% due to the presence of the sensor. This can lead to premature failure of the ice around the gauge and erroneous stress measurements. In addition, if the bond between the gauge and the ice breaks during localized ice failure, the above equations are no longer applicable since the "welded" boundary condition would be violated. Controlled laboratory tests are needed to establish the operational limits of the cylindrical stress sensor.

Determination of ice stresses

The magnitude and direction of the principal stresses in the ice are determined from the measured radial deformation of the sensor in three directions. In the biaxial stress sensor the measurement directions are 120° apart and from eq 7 we have for the displacements of the three wires

$$V_{r_1} = A(p+q) + B(p-q)\cos 2\theta_1 \tag{24}$$

$$V_{r_2} = A(p+q) + B(p-q)\cos 2\theta_2 \tag{25}$$

$$V_{r_3} = A(p+q) + B(p-q)\cos 2\theta_3 \tag{26}$$

where

$$A = \frac{R_2}{8\mu_s}\left[C_2(X_s - 1)\frac{R_c}{R_2} + C_5\frac{R_2}{R_c}\right] \tag{27}$$

$$B = \frac{R_2}{8\mu_s}\left[C_3(X_s - 3)\frac{R_c^3}{R_2^3} + C_7\frac{R_c}{R_2} + C_1(X_s + 1)\frac{R_2}{R_c} + C_4\frac{R_2^3}{R_c^3}\right] \tag{28}$$

$$\theta_2 = \theta_1 + 60° \tag{29}$$

and

$$\theta_3 = \theta_1 + 120°. \tag{30}$$

In the above equations, θ_1 is the angle measured clockwise from principal stress direction p to the measurement direction V_{r1}; $2R_c$ is the average length of the vibrating wires determined from a gauge calibration test. Ideally, A and B should be calculated for each wire; however, all three wires are essentially the same length. All remaining variables have been previously defined.

Solving for p, q and θ, we obtain

$$p = \frac{1}{2}\left[\frac{1}{3B}\left((2V_{r_1} - V_{r_2} - V_{r_3})^2 + 3(V_{r_2} - V_{r_3})^2\right)^{1/2} + \frac{1}{3A}(V_{r_1} + V_{r_2} + V_{r_3})\right] \tag{31}$$

$$q = \left[\frac{1}{3A}(V_{r_1} + V_{r_2} + V_{r_3}) - p\right] \tag{32}$$

and

$$\theta_1 = \frac{1}{2}\cos^{-1}\left[\frac{V_{r_1} - A(p+q)}{B(p-q)}\right] \tag{33}$$

because

$$\cos(\theta) = \cos(-\theta).$$

Equation 33 has two solutions. If

$$V_{r_2} = A(p+q) + B(p-q)\cos 2(\theta_1 + 60°)$$

then θ_1 is positive. If

$$V_{r_2} = A(p+q) + B(p-q)\cos 2(\theta_1 + 120°)$$

then θ_1 is negative.

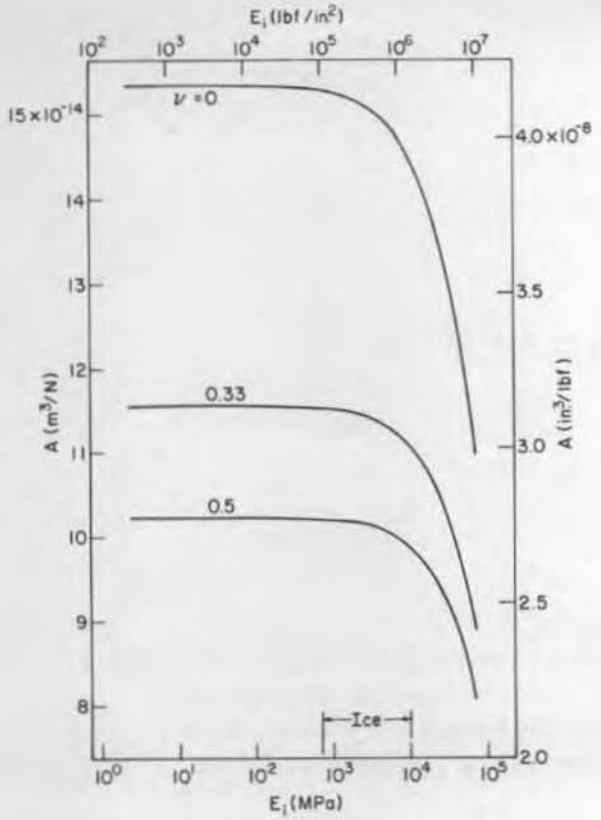

Figure 8. Variation of A *with ice moduli.*

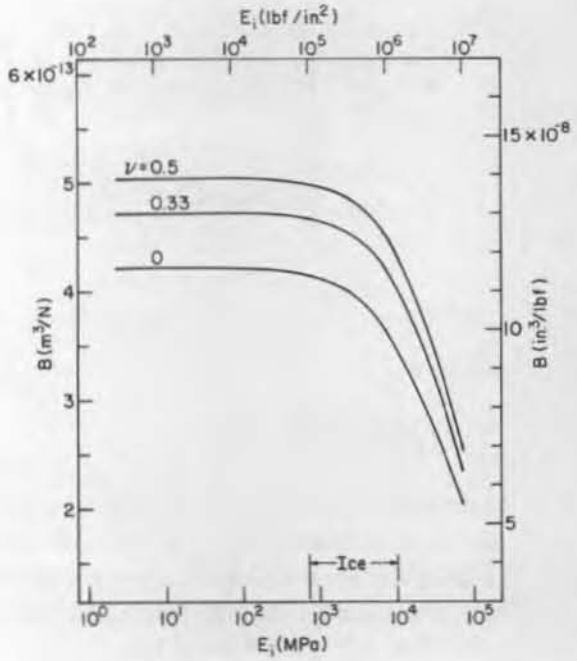

Figure 9. Variation of B *with ice moduli.*

The coefficients A and B depend upon the geometry and mechanical properties of the sensor and the mechanical properties of the surrounding ice. It is desirable to design a cylindrical sensor such that A and B are not greatly affected by variations in the ice mechanical properties. For the biaxial ice stress sensor, R_c was found to be equal to 2.387 ± 0.015 cm. A and B for the biaxial ice stress sensor are plotted against Young's modulus of ice for different Poisson's ratios in Figures 8 and 9 respectively. In the elastic modulus range for ice, A and B show little change with E_i. However, A and B can change significantly with change in ν, Poisson's ratio. Since relatively little is known about Poisson's ratio for ice (Schwarz and Weeks 1977), we assumed a value of 0.33 in this investigation. In the event the ice deforms plastically with $\nu = 0.5$, A and B would then be in error by about 15%. For uniaxial and biaxial ($q/p = 1$) loading conditions, this would result in measured ice stresses that are about 15% too high.

Gauge calibration

The biaxial ice stress sensor is not calibrated in ice. It is calibrated in a hydraulic pressure cell (Fig. 10) to determine the initial frequency and the effective length, $2R_c$, of each vibrating wire. The gauge is radially loaded and the measured deformation of the gauge is compared to the radial deformation of a thick-wall cylinder. The radial deformation of a thick-wall cylinder under external pressure at a radius R_c is given by

$$V_r = \frac{R_2^2\, p}{E_s (R_2^2 - R_1^2)} \left[(1 - \nu_s) R_c + \frac{R_1^2}{R_c} (1 + \nu_s) \right] \tag{34}$$

where R_2 and R_1 are the outer and inner radii of the cylinder, p is the radial hydraulic pressure, and E_s and ν_s are Young's modulus and Poisson's ratio of the sensor material. R_c corresponds

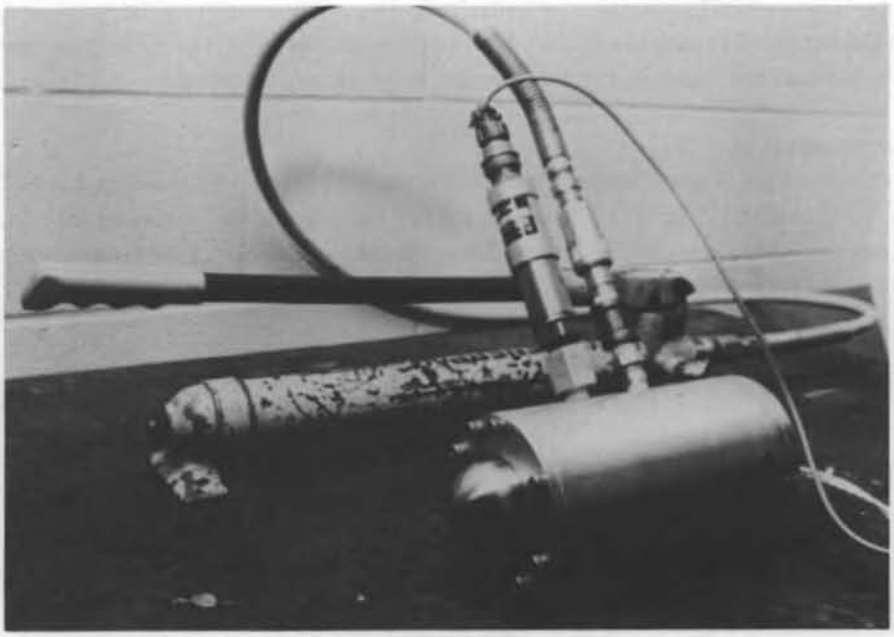

Figure 10. Hydraulic pressure cell used to calibrate the biaxial ice stress sensor.

to the effective radius of the vibrating wire and from eq 2 and 3 we have

$$V_r = - \frac{16 R_c^3 \rho_w}{E_w} \Delta(f^2). \tag{35}$$

From the calibration test we also have the calibration coefficient k_c, which is determined by the least squares method from the test data

$$k_c = \frac{p}{\Delta(f^2)} \tag{36}$$

Combining eq 34, 35 and 36 and noting that

$$E_s = E_w$$

we obtain

$$R_c^4 (16\rho_w) + R_c^2 \left(\frac{k_c R_2^2 (1 - \nu_s)}{R_2^2 - R_1^2} \right) + \frac{R_1^2 R_2^2 k_c (1 + \nu_s)}{R_2^2 - R_1^2} = 0. \tag{37}$$

After determining the effective wire radius, R_c, by trial and error, we can then use eq 35 to accurately obtain the radial deformation of the gauge given the change in vibration frequency of each wire. The average R_c value for all three wires is also used in eq 27 and 28 to calculate A and B.

EVALUATION OF THE BIAXIAL ICE STRESS SENSOR

We conducted controlled laboratory tests to evaluate the biaxial ice stress sensor. The tests were first conducted to determine the temperature sensitivity of the gauge. The sensor was then

frozen into large ice blocks and placed in a biaxial loading machine to study the response of the sensor under different loading conditions. We also examined the effects of differential thermal expansion between the sensor and surrounding ice, and long-term sensor drift.

Temperature sensitivity

We determined the temperature sensitivity of the gauge by placing the sensor in a glycol bath inside an environmental chamber. The temperature of the chamber and bath were varied and sensor readings were taken at different temperatures. The results for each of the three vibrating wires in the gauge are presented in Figure 11.

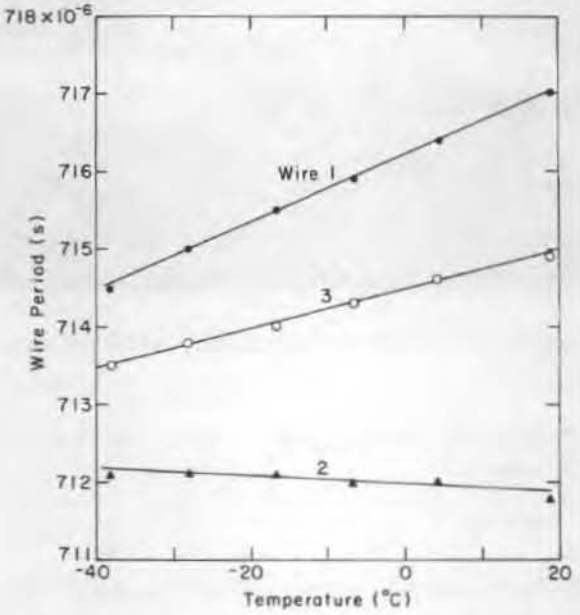

Figure 11. Variation of wire period with temperature for each of the three wires in the biaxial ice stress sensor.

Biaxial loading test equipment

We evaluated the response of the sensor to ice stress by freezing the sensor into large ice blocks and placing the blocks in a hydraulic biaxial loading machine.

The large ice blocks used in these tests were 61 by 61 cm square and 18 cm thick. We chose the length and width of the block to accommodate the entire area of influence of the sensor, about ten diameters (Fig. 5a). The blocks were grown in a coldroom using the freezing chamber shown in Figures 12 and 13. The freezing chamber consisted of a lucite box and coldplate surrounded by foam insulation. To grow an ice block, the box was first filled with either fresh or saline water. An aluminum coldplate was then placed in the top of the box and connected to a glycol constant-temperature bath. The sides of the box and coldplate were then covered with insulation and glycol was pumped through the coldplate. The coldroom was maintained at about 0°C to minimize any growth or melting on the sides of the ice block. Additional details on using this technique to grow ice can be found in Weeks and Cox (1974).

This method of ice growth produces columnar ice which is very similar to that found in natural ice sheets. The grain size of the crystals in the fresh water and saline ice blocks varied between 0.5 and 2.0 cm. The fresh water blocks had both horizontal and vertical c-axis crystals, while the saline ice blocks had predominantly horizontal c-axis crystals. The c-axis of the crystals did not show any preferred alignment in the horizontal plane. A vertical thin section from a fresh water ice block is shown in Figure 14. The saline ice blocks had an average salinity of about 5 °/oo.

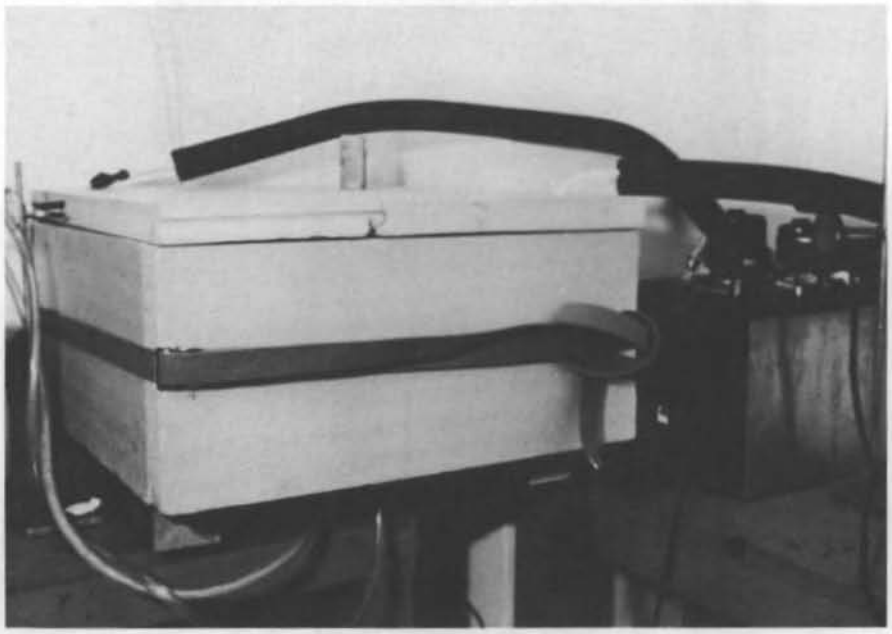

Figure 12. Freezing chamber used to grow ice blocks for the stress sensor verification tests.

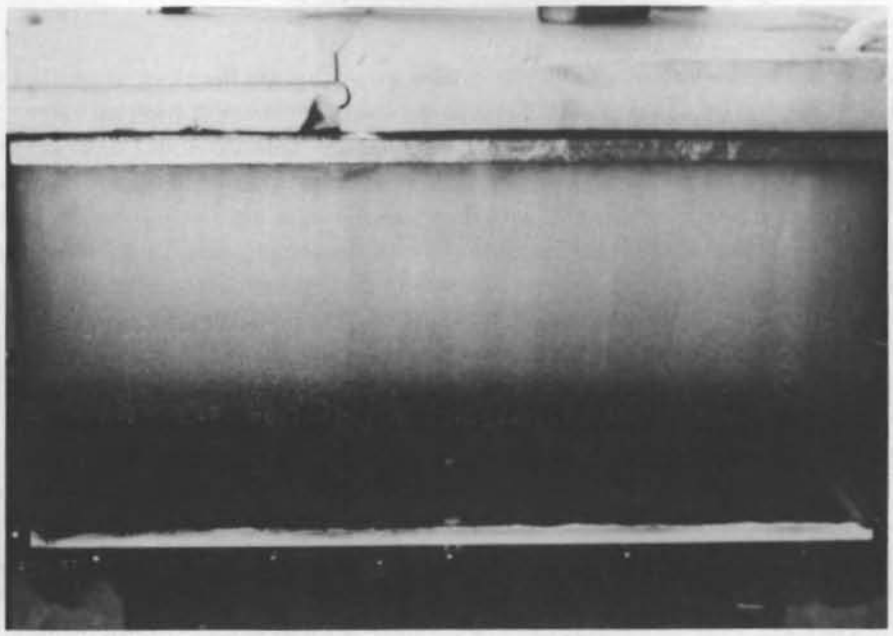

Figure 13. Close-up of freezing chamber showing aluminum coldplate and ice block.

Figure 14. Vertical thin section from fresh water ice block (scale in cm).

The sensor was frozen into an ice block by drilling a hole through the block, supporting the sensor in the hole, and filling the annulus between the sensor and ice with fresh ice water. The center of the block was first found and then a 6.4-cm-diameter hole was drilled through the block with a small auger and electric drill. An extension rod was then attached to the top of the sensor and the sensor was supported in the hole with the frame shown in Figure 15. A rubber gasket was next placed around the bottom of the sensor to close off the annulus between the sensor and ice. After the gasket was in place, ice water was poured into the annulus to freeze the sensor in place. The ice block and sensor temperatures were about -10°C. The next day the support frame and extension rod were removed and the ice block was positioned in the loading machine. After 24 hours, the ice water had frozen and the sensor and ice block temperatures were again at -10°C. Thermal strains in the sensor and ice had also relaxed by that time.

The biaxial loading machine used in the stress sensor verification tests is shown in Figures 16 and 17. The machine consisted of two 0.4-MN-capacity hydraulic rams supported by two independent I-beam frames. The inside ram and frame rolled on casters (Fig. 16) to minimize shear stresses on the block during biaxial loading as well as to compensate for any lack of planar squareness of the ice blocks. The platens consisted of aluminum blocks covered with sheets of Teflon (Fig. 17). They were only 58 cm wide to allow for about 3 cm of block deformation during a test. If the platens were the same width as the ice block (61 cm), the corners of the platens would come into contact during biaxial loading. The platens were also free to rotate in the vertical plane to compensate for any lack of end squareness of the ice blocks.

We applied loads to the ice blocks using the rams and a hydraulic hand pump. We used control valves to direct the hydraulic fluid to one or both rams and a hydraulic dial gauge to measure the

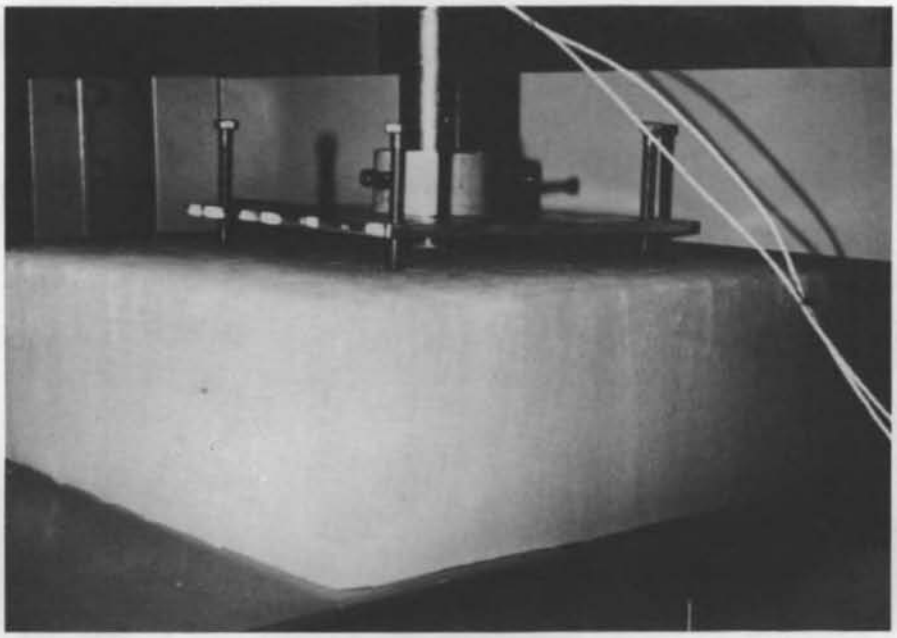

Figure 15. Support frame used to position the sensor in the hole while it was frozen in the ice block.

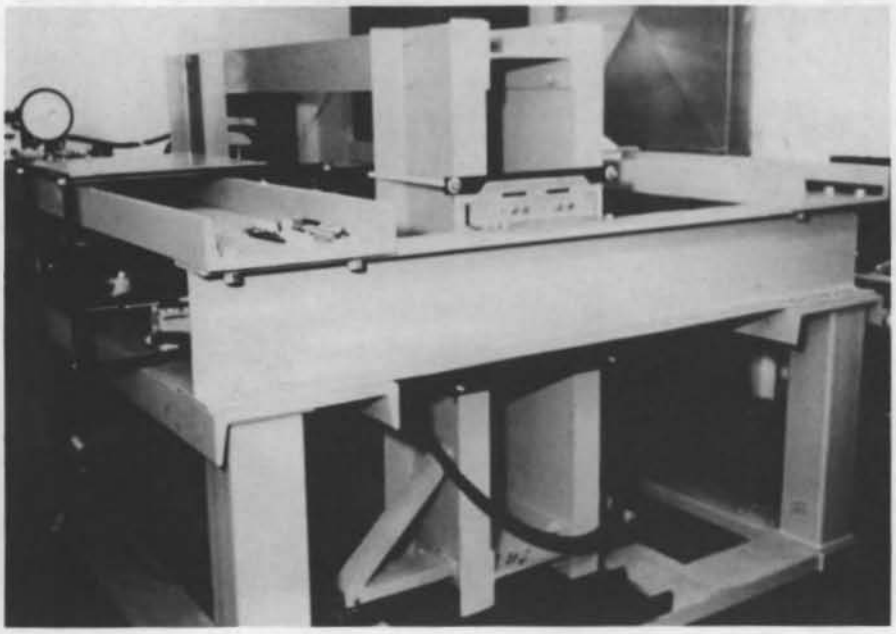

Figure 16. Biaxial loading machine used in stress sensor verification tests.

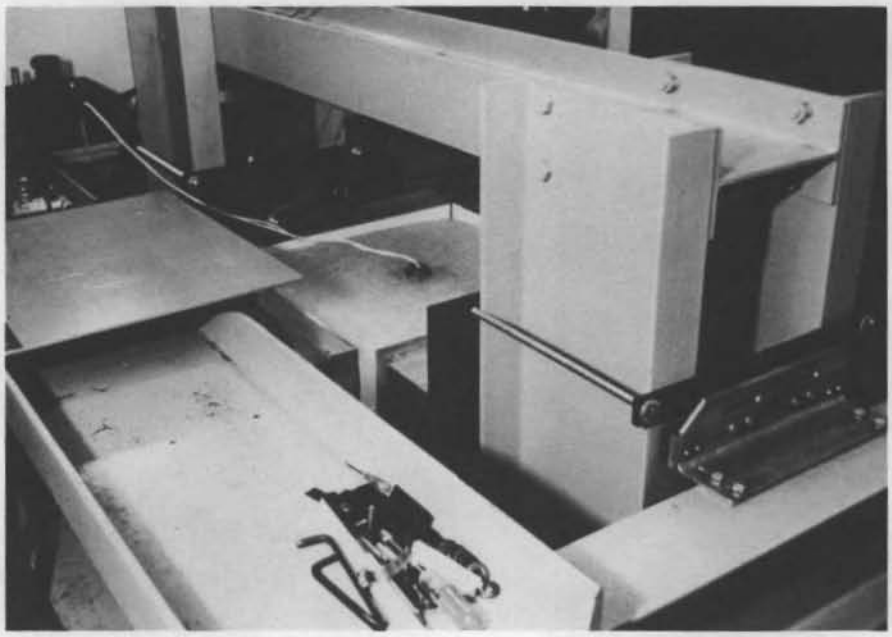

Figure 17. Ice block and sensor in biaxial loading machine.

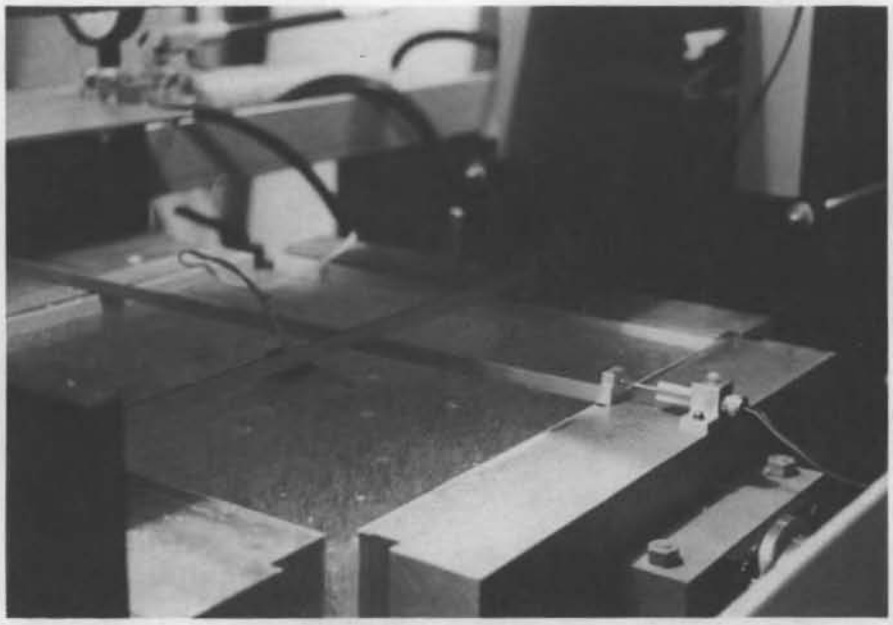

Figure 18. Equipment used to measure block strains during testing.

load. The entire loading system was calibrated with a load cell prior to any testing. Applied uniaxial stresses on the ice blocks had an accuracy of about 20 kPa.

In a few tests, block strains were measured with Direct Current Distance Transducers (DCDTs). The DCDTs were attached to the platens as shown in Figure 18. This equipment was not available for all of the tests.

Biaxial loading test results

We conducted sensor verification tests in both fresh water and saline ice under uniaxial and biaxial loading conditions. A long-term loading test was also performed to evaluate the effects of ice creep on the sensor response. All tests were made at -10°C.

Equations 31 through 33 were used to calculate the magnitude and direction of the principal stresses in the ice from the radial deformation of the gauge. The coefficients A and B were calculated to be equal to 1.152×10^{-13} and 4.739×10^{-13} m^3/N respectively. They were determined from eq 27 and 28, assuming an ice modulus of 0.69 GPa, an ice Poisson's ratio of 0.33 and an effective sensor wire radius, R_c, of 2.387×10^{-2} m. The effective wire radius was determined from the previously described gauge calibration test. We assumed a low value of the ice modulus, in that we expected loading rates on the biaxial loading machine to be relatively small.

Four ice blocks were used in the loading tests. Blocks 1 and 2 were fresh water ice and blocks 3 and 4 were saline ice. The relative position of the sensor to the loading directions in each of the ice blocks is shown in Figure 19. In Figure 19, σ_A, σ_B and τ_{AB} are the applied stresses on the ice block and p and q are the measured principal stresses. We chose the principal stress, p, to be the maximum compressive principal stress. The angle θ is measured clockwise from p to the direction of wire 1 in the sensor. In blocks 3 and 4 we chose wire 1 in the sensor to be parallel to the σ_A or A loading direction.

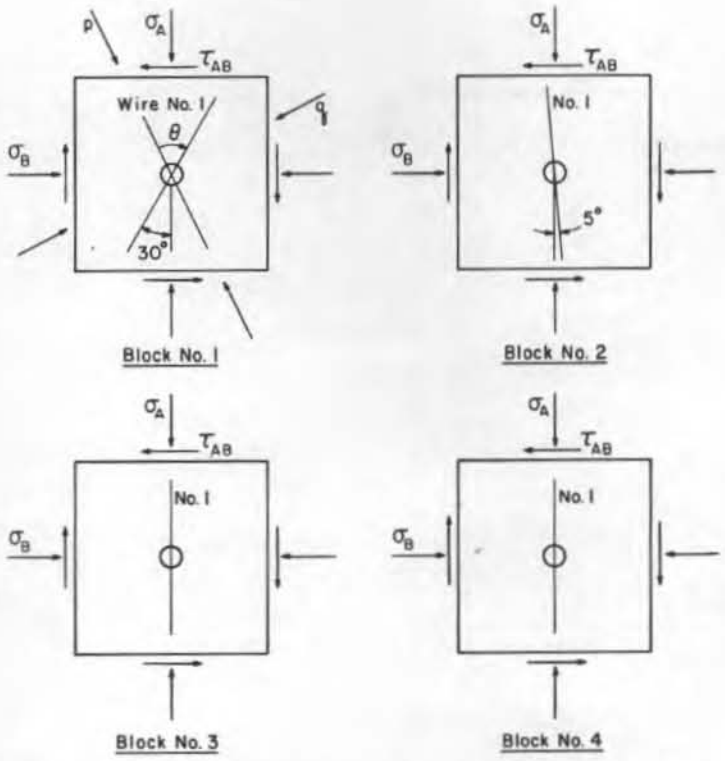

Figure 19. Position of sensor relative to the loading directions for each of the four ice blocks tested.

The loading system was designed to minimize the development of shear stresses on the ice block faces. However, the ice stress readings indicate that small shear stresses (up to 60 kPa) were present on the block faces during the biaxial loading tests. As the applied shear stresses could not be independently measured, it was not possible to compare the applied shear stresses to those measured by the ice stress sensor. In determining the ice stress measurement error, we therefore assumed that the applied shear stresses were zero.

The first ice block used to test the sensor was made from fresh water. The sensor was frozen into the block with wire 1 in the sensor oriented 30° clockwise from the *A* loading direction (Fig. 19). In this first test, the platens were fixed and not free to rotate to compensate for the lack of end squareness. A small load was therefore placed on the block in the *A* direction to cause the ice to creep and come into good contact with the platens. After about 0.24% strain, this was achieved and the block was loaded in the *A* direction in 0.24 MPa increments. The test results are given in Table 1 and plotted in Figure 20. At the conclusion of the test the block was highly fractured and we discarded it.

The second ice block was also made of fresh water ice. The sensor was frozen into the block with wire 1 in the sensor oriented 5° counterclockwise from the *A* loading direction (Fig. 19). Wheelbearing grease was also applied to the platen surfaces to further reduce any shear stresses on the sides of the block. We used this block to examine the sensor response under both uniaxial and biaxial loads ($\sigma_A = \sigma_B$) as well as to changes in direction of the applied stress. Since the platens were still not free to rotate, a biaxial load was first applied to the ice to cause the ice to creep and come into good contact with the platens. Once reasonable contact was obtained, the ice was loaded equally in the *A* and *B* directions, then only in the *B* direction and finally in the *A* direction. The results are given in Table 2 and plotted in Figure 21. Since small shear stresses can be present on the block loading faces when biaxially loaded, measured loads σ_A, σ_B and τ_{AB} were derived from p, q and θ using Mohr circle theory.

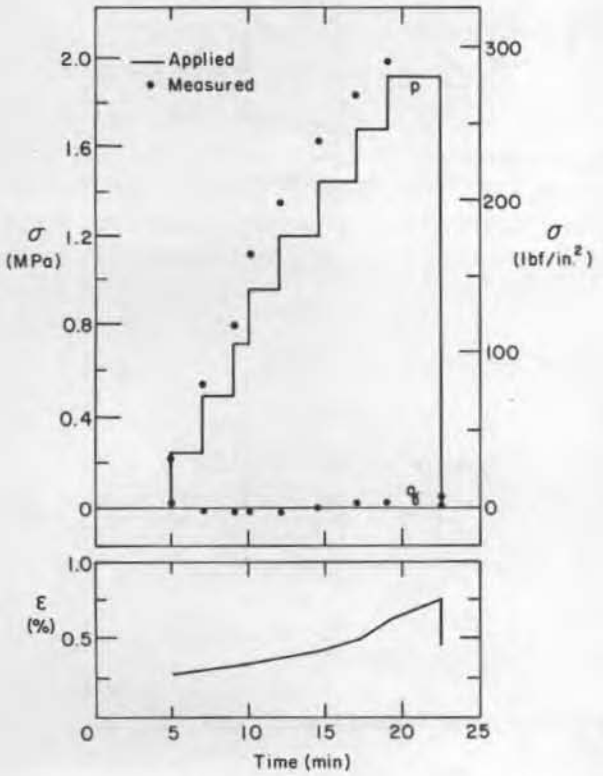

Figure 20. Measured stress versus applied stress and block strain for block 1.

Table 1. Comparison of applied and measured stress data for block 1.

Time (min)	Applied stress σ_A (MPa)	Applied stress σ_B (MPa)	Measured stress p (MPa)	Measured stress q (MPa)	Measured stress θ (degrees)	Strain ϵ (%)	Maximum error (MPa)	Maximum error (%)
0	0	0	0	0	0	0	0	0
5	0.24	0	0.23	0.01	29	0.24	0.01	6
7	0.48	0	0.54	-0.01	28	0.27	0.06	13
9	0.72	0	0.81	-0.02	27	0.32	0.08	11
10	0.97	0	1.12	-0.02	27	0.35	0.15	16
12	1.21	0	1.37	-0.01	26	0.38	0.16	13
14	1.45	0	1.63	0	26	0.43	0.19	13
17	1.69	0	1.84	0.01	24	0.51	0.15	9
19	1.93	0	2.00	0.03	24	0.64	0.07	4
25	0	0	0.04	0.01	10	0.48	0.04	-

Table 2. Comparison of applied and measured stress data for block 2.

Time (min)	Applied stress σ_A (MPa)	Applied stress σ_B (MPa)	Measured stress p (MPa)	Measured stress q (MPa)	Measured stress θ (degrees)	σ_A (MPa)	σ_B (MPa)	τ_{AB} (MPa)	Maximum error (MPa)	Maximum error (%)
0	0	0	0	0	0	0	0	0	0	-
3	0.23	0.23	0.24	0.22	56	0.23	0.23	-0.01	0.01	0
6	0.46	0.46	0.50	0.48	54	0.48	0.49	-0.01	0.03	6
9	0.69	0.69	0.74	0.70	82	0.70	0.74	0	0.06	8
11	0	0	0.02	0.01	81	0.01	0.02	0	0.02	-
27	0	0	0.01	0	60	0	0.01	0	0.01	-
28	0	0.23	0.25	-0.03	85	-0.03	0.25	0	0.03	12
29	0	0.46	0.50	-0.05	84	-0.05	0.50	-0.01	0.05	10
31	0	0.69	0.78	-0.09	84	-0.09	0.78	-0.01	0.09	13
46	0	0	0.01	0.01	45	0.01	0.01	0	0.01	-
47	0.23	0	0.26	-0.01	-3	0.26	-0.01	-0.01	0.03	12
49	0.46	0	0.54	-0.03	-5	0.54	-0.03	0	0.08	16
51	0.69	0	0.79	-0.06	-8	0.79	-0.06	0.03	0.10	15

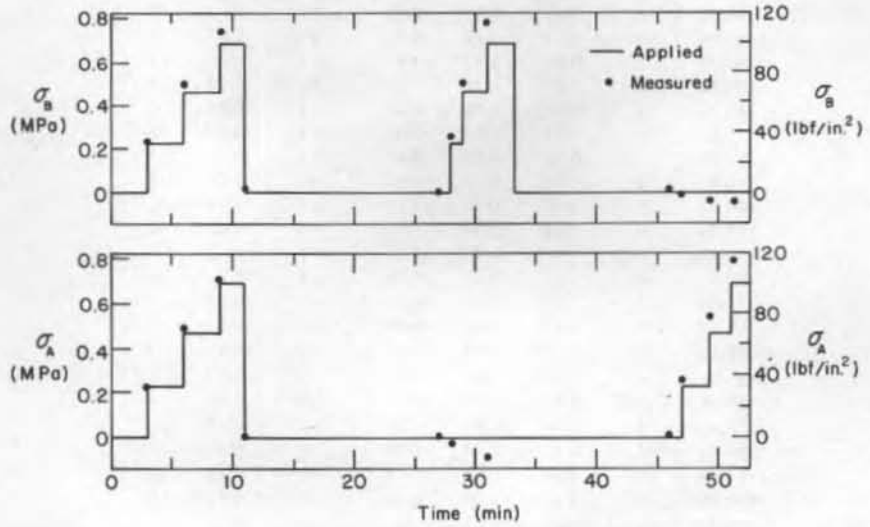

Figure 21. Measured versus applied stress in the A *and* B *directions for block 2.*

Table 3. Comparison of applied and measured stress data for block 3.

Time	Applied stress σ_A	Applied stress σ_B	Measured stress p	Measured stress q	Measured stress θ	Maximum error	
(hours)	(MPa)	(MPa)	(MPa)	(MPa)	(degrees)	(MPa)	(%)
0.00	0	0.46	0.54	-0.03	-89	0.08	15
0.40	0	0.46	0.52	-0.02	-89	0.06	14
0.98	0	0.39	0.44	-0.03	-89	0.06	14
1.03	0	0.46	0.52	-0.02	-89	0.07	15
2.70	0	0.26	0.28	-0.03	-90	0.03	11
2.88	0	0.46	0.49	-0.03	-89	0.03	8
3.33	0	0.32	0.37	-0.03	-90	0.05	15
3.35	0	0.46	0.51	-0.03	-89	0.06	12
17.83	0	0.14	0.14	-0.03	89	0.03	24
17.90	0	0.46	0.44	-0.02	90	0.02	5
23.45	0	0.23	0.21	-0.03	89	0.03	12
23.48	0	0.46	0.45	-0.03	90	0.03	6
26.92	0	0.27	0.25	-0.03	89	0.03	13
47.23	0	0.19	0.17	-0.03	88	0.03	15
47.25	0	0.46	0.43	-0.01	89	0.03	6
51.02	0	0.28	0.27	-0.03	89	0.03	10
51.05	0	0.46	0.46	-0.01	89	0.01	2
75.55	0	0.23	0.17	-0.03	88	0.06	24
75.68	0	0.46	0.43	0	89	0.03	6
89.82	0	0.26	0.23	-0.02	88	0.03	11
89.88	0	0.46	0.44	-0.01	88	0.01	3
95.15	0	0.32	0.30	-0.01	88	0.02	6
95.18	0	0.46	0.46	0	89	0	0
98.67	0	0.35	0.34	0	88	0.01	2
98.68	0	0.46	0.46	-0.01	88	0.01	2
115.53	0	0.28	0.29	-0.01	87	0.01	2
115.57	0	0.46	0.47	0.01	88	0.01	3
119.12	0	0.37	0.37	0.01	87	0.01	4
119.17	0	0.46	0.47	0.01	87	0.01	3
123.55	0	0.39	0.40	0.01	87	0.01	4
123.60	0	0.46	0.49	0.02	87	0.03	8
137.77	0	0.34	0.37	0.03	87	0.03	8
137.82	0	0.46	0.48	0.02	87	0.02	5
142.50	0	0.46	0.48	0.03	87	0.03	6
142.55	0	0	0.05	-0.03	15	0.05	-
142.98	0	0	0.01	-0.05	14	0.05	-
144.07	0	0	0.01	-0.02	33	0.02	-
145.35	0	0	-0.01	-0.03	41	0.03	-
146.08	0	0	0.01	-0.03	41	0.03	-
146.20	0	0.46	0.48	-0.03	41	0.03	5
147.68	0	0.28	0.29	-0.03	89	0.03	10
147.72	0	0.46	0.47	-0.03	89	0.03	6
163.26	0	0.19	0.18	-0.03	-89	0.03	14
163.30	0	0.46	0.43	-0.03	-89	0.03	6
168.20	0	0.28	0.26	-0.03	-89	0.03	8
168.21	0	0.46	0.45	-0.01	-89	0.01	3
171.85	0	0.29	0.27	-0.03	-89	0.03	10
171.88	0	0.46	0.44	-0.02	-89	0.02	5
190.71	0	0.23	0.18	-0.02	-89	0.04	18
190.75	0	0.46	0.43	-0.01	-89	0.02	5
191.06	0	0.37	0.37	-0.02	-89	0.02	6
191.11	0	0	-0.03	-0.03	-59	0.03	-
192.11	0	0	-0.01	-0.03	-26	0.03	-
194.51	0	0	-0.01	-0.03	-42	0.03	-
195.13	0	0.32	0.30	-0.03	-89	0.03	9
195.16	0	0.46	0.48	-0.02	-90	0.02	5
195.26	0	0.68	0.68	-0.03	-90	0.03	4
195.30	0	0.91	0.90	-0.03	-90	0.03	4
195.38	0	1.14	1.05	-0.03	-90	0.08	7
195.41	0	1.37	1.48	0.08	-90	0.12	9
195.45	0	1.59	1.79	0.25	-89	0.25	16
195.48	0	1.82	2.08	0.32	-89	0.32	18
195.53	0	0	0.03	0	-19	0.03	-
196.21	0	0	-0.01	-0.03	-34	0.03	-

The third ice block was made of saline ice. The sensor was frozen into the block with wire 1 in the sensor oriented parallel to the *A* loading direction (Fig. 19). Wheelbearing grease was not applied to the platen surfaces as we regarded it as being too messy. However, the platens were modified and now were free to rotate and compensate for lack of end squareness. We used block 3 to examine the effects of ice creep on the sensor. At the end of the creep test, the block was uniaxially loaded until it could no longer sustain the load. The test results are given in Table 3 and plotted in Figure 22. Due to ice creep, a constant load could not be maintained on the ice block; therefore the load was adjusted to its initial value each time a stress reading was taken.

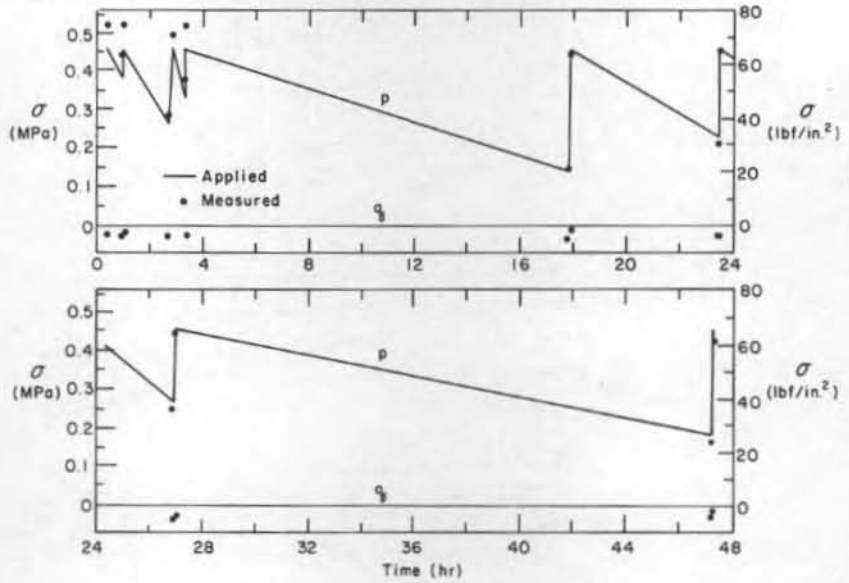

a. 0 to 48 hours.

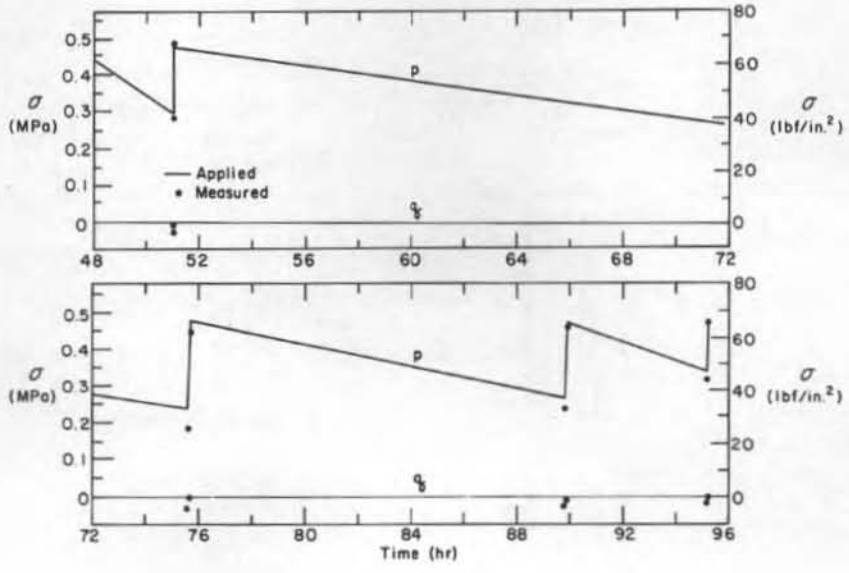

b. 48 to 96 hours.

Figure 22. Measured versus applied stress for block 3.

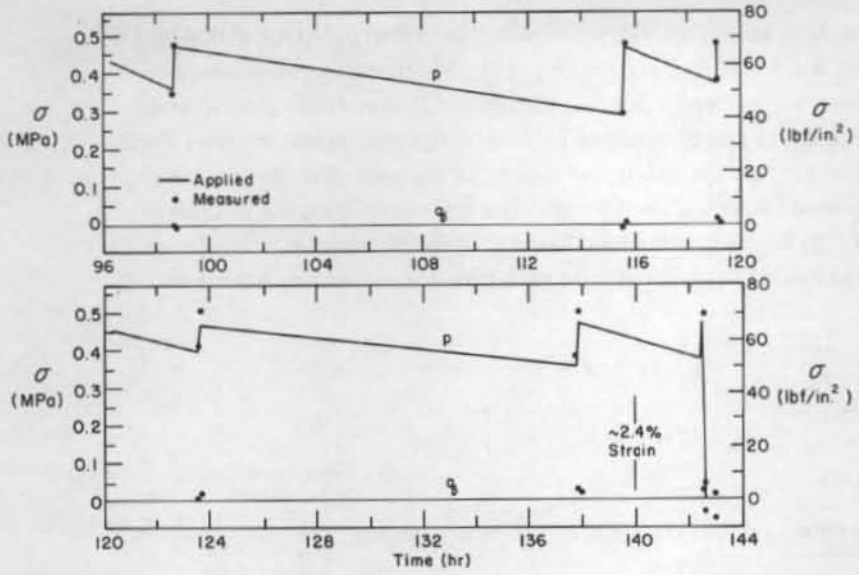

c. 96 to 144 hours.

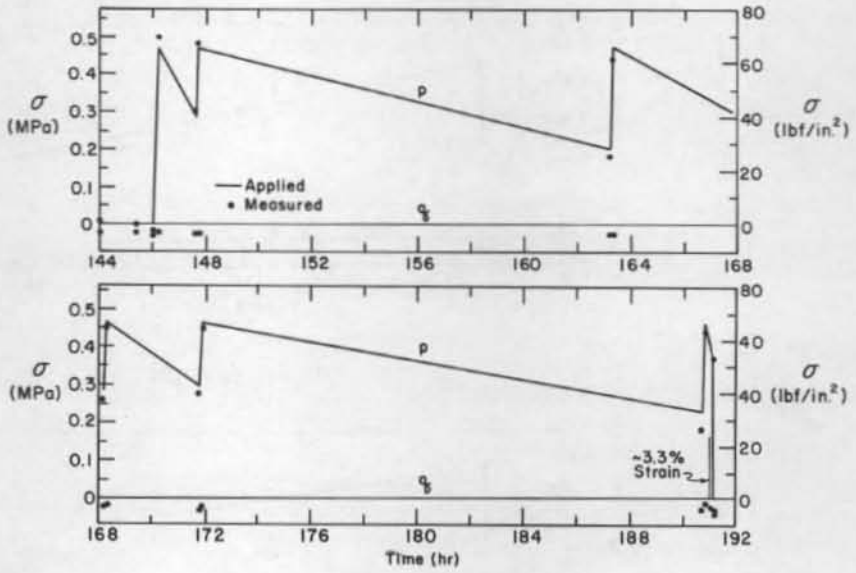

d. 144 to 192 hours.

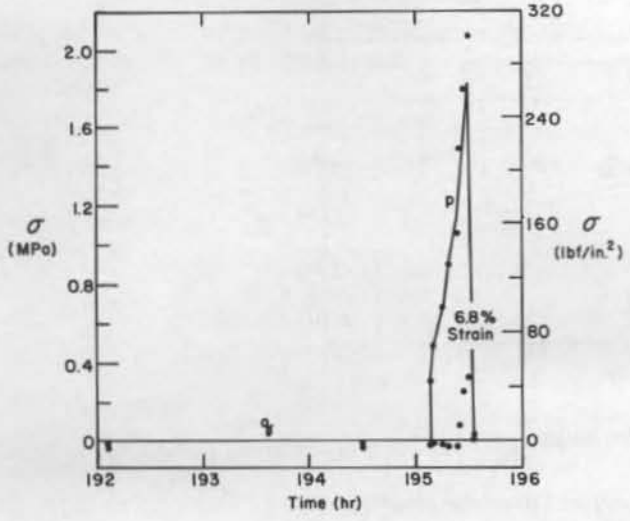

e. 192 to 196 hours.

Figure 22 (cont'd). Measured versus applied stress for block 3.

The fourth and last ice block was also made of saline ice. The sensor was frozen into the block with wire 1 in the sensor oriented parallel to the *A* loading direction. We used block 4 to evaluate the response of the sensor under biaxial loads where the applied loads σ_A and σ_B were not equal. Such tests are difficult in that lateral strains cause the ice to bow out in the minor loading direction, degrading the squareness of the block. The test results are given in Table 4 and are plotted in Figure 23. Again, measured stresses in the loading directions are compared to the applied stresses as small shear stresses develop on the platens during biaxial loading.

Table 4. Comparison of applied and measured stress data for block 4.

	Applied stress		*Measured stress*						*Maximum error*	
Time	σ_A	σ_B	p	q	θ	σ_A	σ_B	τ_{AB}		
(min)	*(MPa)*	*(MPa)*	*(MPa)*	*(MPa)*	*(degrees)*	*(MPa)*	*(MPa)*	*(MPa)*	*(MPa)*	*(%)*
0.00	0	0	0	0	0	0	0	0	0	0
0.03	0	0.23	0.23	0.05	-90	0.05	0.23	0	0.05	21
0.12	0	0.23	0.24	0.04	-89	0.04	0.24	0.01	0.04	18
0.27	0	0.23	0.25	0.03	-88	0.03	0.25	0.01	0.03	15
0.30	0.23	0.23	0.19	0.14	69	0.14	0.18	-0.01	0.09	38
0.42	0.23	0.23	0.19	0.16	50	0.17	0.18	-0.01	0.06	26
0.52	0.23	0.23	0.19	0.16	48	0.17	0.17	-0.01	0.06	26
0.58	0.23	0.23	0.20	0.17	40	0.19	0.19	-0.01	0.05	21
0.67	0.23	0.48	0.45	0.16	85	0.16	0.45	-0.03	0.08	32
0.80	0.23	0.48	0.48	0.15	85	0.15	0.48	-0.03	0.08	35
0.88	0.23	0.48	0.47	0.16	83	0.17	0.46	-0.03	0.07	29
0.98	0.23	0.48	0.48	0.16	81	0.17	0.48	-0.05	0.07	29
1.03	0.48	0.48	0.49	0.40	55	0.43	0.46	-0.04	0.03	7
1.18	0.48	0.48	0.48	0.40	46	0.43	0.44	-0.03	0.04	9
1.28	0.48	0.48	0.50	0.42	42	0.46	0.46	-0.03	0.03	4
1.38	0.71	0.48	0.74	0.42	7	0.74	0.43	-0.04	0.05	10
1.43	0.71	0.48	0.73	0.43	7	0.72	0.44	-0.04	0.03	7
1.48	0.71	0.71	0.72	0.63	28	0.70	0.64	-0.04	0.07	10
1.63	0.71	0.71	0.73	0.64	30	0.71	0.66	-0.04	0.05	7
1.68	0.71	0.94	0.94	0.68	79	0.68	0.93	-0.05	0.03	4
1.85	0.71	0.94	0.94	0.68	79	0.68	0.94	-0.05	0.03	4
1.88	0.94	0.94	1.01	0.91	38	0.97	0.94	-0.05	0.03	3
2.00	0.94	0.94	1.01	0.90	30	0.98	0.93	-0.04	0.03	4
2.03	0	0	0.02	0.01	0	0.02	0.01	-0.04	0.02	-
2.18	0	0	0.02	0.01	0	0.02	0.01	0	0.02	-
2.25	0.48	0.48	0.48	0.39	23	0.47	0.40	-0.03	0.08	16
2.38	0.48	0.48	0.50	0.41	23	0.48	0.42	-0.03	0.06	12
2.45	0.48	0.94	0.99	0.45	84	0.46	0.98	-0.06	0.03	4
2.52	0.48	0.94	0.97	0.47	84	0.48	0.97	-0.06	0.02	2
2.55	0.94	0.94	0.98	0.90	30	0.96	0.92	-0.03	0.02	2
2.72	0.94	0.94	0.99	0.90	23	0.98	0.91	-0.03	0.03	4
2.78	0	0	0.03	0.01	3	0.03	0.01	-0.01	0.03	-
2.87	0	0	0.02	0.01	0	0.02	0.01	0	0.02	-
2.95	0	0	0.02	0.01	0	0.02	0.01	0	0.02	-
3.00	0.48	0.48	0.48	0.38	25	0.46	0.40	-0.04	0.08	16
3.17	0.48	0.48	0.50	0.41	24	0.49	0.42	-0.03	0.06	12
3.22	0.94	0.48	1.01	0.41	3	1.01	0.41	-0.03	0.07	17
3.28	0.94	0.48	1.04	0.47	3	1.04	0.47	-0.03	0.10	10
3.33	0.94	0.48	0.01	0.48	3	1.01	0.48	-0.03	0.06	7
3.47	0	0	0.03	0.01	6	0.03	0.01	0	0.03	-
3.52	0	0	0.02	0.01	0	0.02	0.01	0	0.02	-

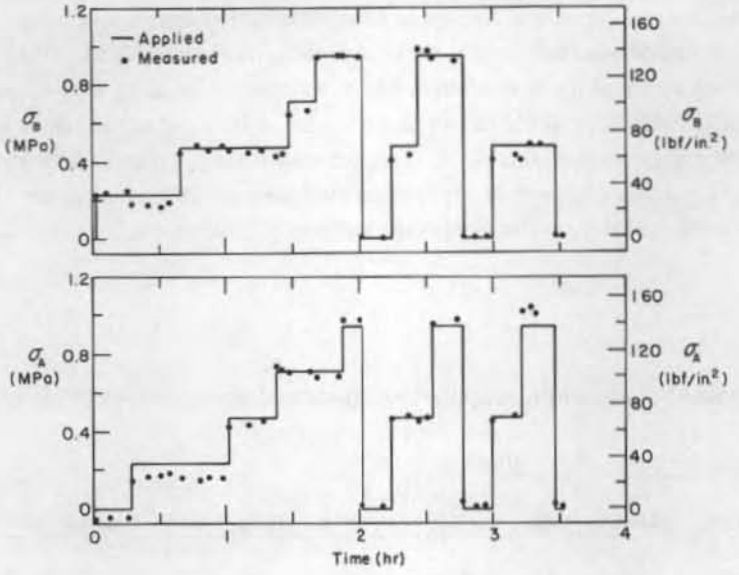

Figure 23. Measured versus applied stress for block 4.

Differential thermal expansion

We also used block 4 to study the effects of differential thermal expansion between the ice and gauge. To simulate conditions in the field where the sensor would be covered with an insulated instrument box, the block was insulated on the top and bottom with foam. The temperatures of the sensor and block were then varied from -20°C to 0°C and back to -10°C to examine the response of the gauge. After the stress measurements were corrected for changes in temperature, the stress readings were generally within or equal to the resolution of the sensor, 20 kPa.

Long-term drift

During the course of the evaluation study, sensor readings were obtained at 20°C to examine the stability of the unloaded gauge. The period of vibration of each of the three wires in the gauge

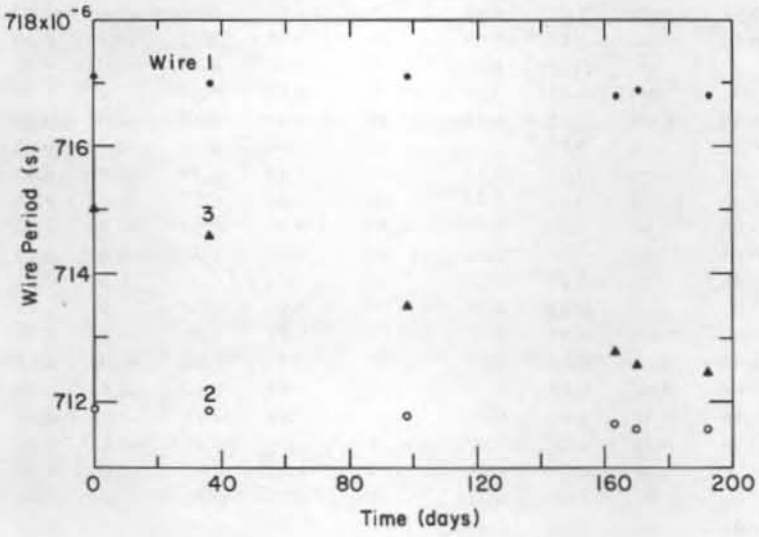

Figure 24. Variation of wire period with time for each of the three wires in the biaxial ice stress sensor.

is plotted against time in Figure 24. Over a period of about 200 days wires 1 and 2 showed a slight decrease in the wire period, while wire 3 showed a significant change.

Discussion of test results

The biaxial ice stress sensor has a low temperature sensitivity and the sensor response is not affected by differential thermal expansion between the ice and gauge.

The sensor output appears to vary linearly with temperature. If the sensor were in ice, the observed changes in output would correspond to stresses of about 5 kPa/°C. Relative to the resolution of the gauge (20 kPa), the temperature sensitivity is small. In many short-term applications of the gauge, temperature corrections would not be needed. However, in situations where large variations in ice temperature did occur, the sensor output would have to be corrected to obtain the highest possible accuracy.

Metge et al. (1975) postulated that the response of a steel ice stress sensor would be greatly affected by differential thermal expansion between the ice and gauge. However, the results of this investigation and those of Johnson and Cox (1980) do not support this hypothesis. If ice were an elastic material, differential thermal expansion would be a problem. Because ice creeps under low stress, localized thermal stresses in the ice around the sensor rapidly relax and are unable to build up to any significant value.

The results of the loading tests indicate that the sensor responds immediately to applied loads. In general, measured stresses are within 15% of the applied stresses for both uniaxial and biaxial loading. The sensor response does not appear to be affected by ice creep and when the applied stresses are removed, the measured stresses fall close to zero. Reliable stress measurements are also obtained well beyond yielding or failure of the ice. In addition, the sensor can usually determine the direction of the applied stresses to within 5°.

Part of the observed error can be attributed to the resolution of the gauge (20 kPa) and the loading system (20 kPa). Combined, they account for about 30 kPa of the observed differences in the applied and measured stress. These differences are significant at low stress levels. Errors are also introduced by poor seating between the sides of the ice block and platens, and shear stresses on the block sides during biaxial loading. The block 3 and block 4 results show that stress measurements improve significantly when the applied stresses are held constant on the block.

If it were possible to solve the seating and shear stress problems associated with the loading machine, measured stresses would probably be within 10% of the applied stresses. This postulate is supported by the results from block 3 where a uniaxial load was maintained on the ice block. After about 3 hours, the block appears to be properly seated and the difference between the applied and measured stress is less than or equal to the combined error associated with the resolution of the gauge and loading system. Since a biaxial field can be described as the superposition of two normal uniaxial fields, the same results should be observed in a well-designed biaxial loading test where problems associated with poor seating, bulging of the ice block and shear stresses have been eliminated.

Periodic measurements under no load reveal that the sensor exhibits long-term drift. With time the strain in the vibrating wires increases, resulting in a decrease in the wire period. According to IRAD Gage, the gauge fabricator, this behavior is caused by outward displacement of the clamps holding the wires in the sensor. Work on borehole stressmeters indicates that the problem can be eliminated by heat-treating the sensor after fabrication. This was not done for the prototype sensor.

CONCLUSIONS

Reliable ice stress measurements can be obtained by measuring the diametral deformation of a stiff steel cylinder embedded in the ice. By measuring the deformation of the cylinder in three

directions, we can determine both the magnitude and direction of the principal stresses in the ice. Analytical solutions describing the behavior of an elastic ring welded in an elastic plate adequately predict the sensor's inclusion factor (stress concentration factor) in ice, despite the fact that ice is a time-dependent material. Since the sensor is considerably stiffer than the ice, its deformation is not significantly affected by variations in the ice elastic modulus and by nonelastic behavior. It is not necessary to calibrate the sensor in ice.

Our controlled laboratory experiments to evaluate the biaxial ice stress sensor indicate that the sensor has a low temperature sensitivity (5 kPa/°C) and is not significantly affected by differential thermal expansion between the ice and the gauge. Loading tests on fresh water and saline ice blocks containing an embedded sensor show that the sensor has a resolution of 20 kPa and an accuracy of better than 15% under a variety of both uniaxial and biaxial load conditions. When allowances are made for poor seating of the ice blocks in the loading machine and shear stresses on the platens, test results suggest that the sensor accuracy may be better than 10% of the applied stress. Principal stress directions can be resolved to within about 5°.

The cylindrical sensor does not greatly overload the ice and can accurately measure ice stresses well beyond ice yielding or failure. The maximum stress riser produced by the presence of the sensor in the ice is about 1.5.

The sensor is also rugged, leak-proof, and can be easily installed in an ice sheet with conventional augering equipment.

LITERATURE CITED

Baumann, W.A. (1979) In-situ stress measurements in a fresh water ice sheet. M.S. Thesis. Milwaukee: University of Wisconsin.

Berry, D.S. and C. Fairhurst (1966) Influence of rock anisotropy and time dependent deformation of the stress-relief and high modulus inclusion techniques of in situ stress determination. *Testing Techniques for Rock Mechanics.* ASTM STP 402. Philadelphia: American Society for Testing and Materials, pp. 190–206.

Buswell, H.J., D.R. Moore and A. Owens (1975) Solid inclusion stress gage in composite propellant charges. *Journal of Spacecraft and Rockets,* **12**(9): 465–471.

Chen, A.C.T. (1981a) Ice pressure sensor inclusion factors. *ASME Journal of Energy Resources Technology,* **103**: 82–86.

Chen, A.C.T. (1981b) Transverse pressure effects on an embedded ice pressure sensor. In *Proceedings of the Sixth International Conference on Port and Ocean Engineering under Arctic Conditions (POAC '81), July 27–31, Quebec City, Canada.* Vol. 1, pp. 375–384.

Chen, A.C.T. and J.S. Templeton (1983) Field in-ice pressure sensor response tests. *ASME Journal of Energy Resources Technology,* **105**: 6–11.

Frederking, R. (1980) A tubular transducer for in-situ stress measurements in ice. In *Proceedings of the Workshop on Sea Ice Field Measurements, St. John's, Newfoundland.* Centre for Cold Ocean Resources Engineering, C-CORE Report 80-21, pp. 165–192.

Halliday, D. and R. Resnick (1970) *Fundamentals of Physics.* New York: John Wiley and Sons.

Hawkes, I. (1969a) Stress evaluation in low-modulus and viscoelastic materials using photoelastic inclusions. *Experimental Mechanics,* **9**(2): 58–66.

Hawkes, I. (1969b) Biaxial stress and strain measurements using photoelastic hollow cylinder inclusion meters. USA Cold Regions Research and Engineering Laboratory, Special Report 133.

Hawkes, I. and W.V. Bailey (1973) Design, develop, fabricate, test and demonstrate permissible low cost cylindrical stress gauges and associated components capable of measuring change of stress as a function of time in underground coal mines. U.S. Bureau of Mines Contract Report H0220050, NN.

Hawkes, I. (1975) Letter from IRAD Gage to Sun Oil, 21 November.

Johnson, J.B. and G.F.N. Cox (1980) The OSI ice stress sensor. In *Proceedings of the Workshop on Sea Ice Field Measurements, St. John's, Newfoundland.* Centre for Cold Ocean Resources Engineering, C-CORE Report 80-21, pp. 193–207.

Johnson, J.B. and G.F.N. Cox (1982) Stress sensor particularly suited for elastic, plastic, and viscoelastic materials. United States Patent 4,346,600, 31 August.

Metge, M., A. Strilchuk and P. Trofimenkoff (1975) On recording stresses in ice. In *Proceedings, IAHR Third International Symposium on Ice Problems, 18–21 August, Hanover, New Hampshire.* USA Cold Regions Research and Engineering Laboratory, pp. 459–468.

Nelson, R.D. and W.M. Sackinger (1976) Stresses in sea ice. ASME Joint Petroleum Mechanical Engineering and Pressure Vessels and Piping Conference, Mexico City.

Nelson, R.D., M. Tauriainen and J. Borghorst (1977) Techniques for measuring stress in sea ice. University of Alaska. Alaska Sea Grant Report, No. 77-1.

Sackinger, W.M. and R.D. Nelson (1979a) Ice stresses near grounded structures. In *Proceedings, Fifth International Conference on Port and Ocean Engineering under Arctic Conditions (POAC '79), 13–18 August, Trondheim, Norway.* Vol. 1. Norwegian Institute of Technology, pp. 57–72.

Sackinger, W.M. and R.D. Nelson (1979b) Sea ice stresses near grounded obstacles. In *Proceedings, 1979 Offshore Technology Conference, 30 April–3 May, Houston, Texas.* Vol. 3, pp. 1495–1502.

Savin, G.N. (1961) *Stress Concentrations Around Holes.* New York: Pergamon Press.

Schwarz, J. and W.F. Weeks (1977) Engineering properties of sea ice. *Journal of Glaciology,* **19**(81): 499–531.

Skilton, D. (1971) Behavior of rigid inclusion stress meters in viscoelastic rock. *International Journal of Rock Mechanics and Mining Science,* **8**: 283–289.

Suzuki, S. (1969) Stress measurements in an infinite plate with a hole reinforced by different materials. *Experimental Mechanics,* **9**(2): 332–336.

Templeton, J.S. (1979) On measurement of sea ice pressures. In *Proceedings, Fifth International Conference on Port and Ocean Engineering under Arctic Conditions (POAC '79), 13–18 August, Trondheim, Norway.* Vol. 1. Norwegian Institute of Technology, pp. 73–88.

Templeton, J.S. (1981) Analysis for an embedded ice pressure sensor. *ASME Journal of Energy Resources Technology,* **103**: 87–95.

Traetteberg, A., L.W. Gold and R. Frederking (1975) The strain rate and temperature dependence of Young's modulus of ice. In *Proceedings, IAHR Third International Symposium on Ice Problems, 18–21 August, Hanover, New Hampshire,* USA Cold Regions Research and Engineering Laboratory, pp. 479–486.

Vaudrey, K.D. (1977) Ice engineering–Study of related properties of floating sea ice sheets and summary of elastic and viscoelastic analyses. Naval Civil Engineering Laboratory Technical Report R860.

Weeks, W.F. and G.F.N. Cox (1974) Laboratory preparation of artificial sea and salt ice. USA Cold Regions Research and Engineering Laboratory, Special Report 206.

Williams, F.T. (1973) The behavior of stress measuring devices in rocks of various materials. In *Field Instrumentation in Geotechnical Engineering, A Symposium held 30 May–1 June 1973.* New York: John Wiley and Sons, pp. 462–474.

Wilson, A.H. (1961) A laboratory investigation of a high modulus borehole plug gage for the measurement of rock stress. In *Proceedings of the 4th Symposium on Rock Mechanics, 30 March–1 April, University Park* (H.L. Hartman, Ed.). University Park: Pennsylvania State University, Bulletin of the Mineral Industries Experimental Station, pp. 185–195.